MATHEMATICAL MODELING OF CENTRIFUGAL CASTING OF METAL MATRIX COMPOSITE

A DISSERTATION

Submitted in partial fulfilment of the requirements for the award of the degree of

MASTER OF TECHNOLOGY

in

METALLURGICAL AND MATERIALS ENGINEERING

(With Specialization in Industrial Metallurgy)

By

PRAVEEN KUMAR PATEL

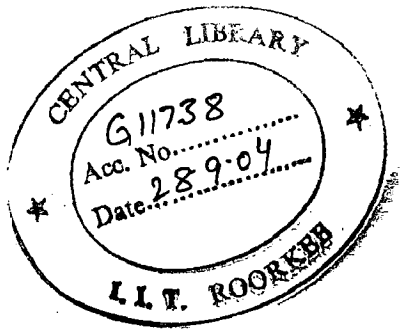

DEPARTMENT OF METALLURGICAL AND MATERIALS ENGINEERING
INDIAN INSTITUTE OF TECHNOLOGY ROORKEE
ROORKEE-247 667 (INDIA)

NOVEMBER, 2003

CANDIDATE'S DECLARATION

I hereby certify that the work, which is presented in the dissertation entitled **"MATHEMATICAL MODELING OF CENTRIFUGAL CASTING OF METAL MATRIX COMPOSITE"**, in partial fulfillment for the award of the degree of **MASTER OF TECHNOLOGY** in ***Industrial Metallurgy,*** submitted in ***Department of Metallurgical and Materials Engineering, I.I.T. Roorkee***, is an authentic record of my own work carried out for a period of Nine months from January 2003 to September 2003 under the supervision of **Dr. Satya Prakash**, Professor, Department of Metallurgical and Materials Engineering, I.I.T Roorkee, and **Mr. K.S Ramaswamy**, Sr. Manager, (R&M), NTPC/NCPS, Dadri, Gautam Budha Nagar, (UP).

I have not submitted the matter of the present dissertation for the award of any other degree.

Place: Roorkee
Date: 10/11/2003

Praveen Kumar Patel
(PRAVEEN KUMAR PATEL)

This is to certify that the above statement made by the candidate is correct to the best of my knowledge.

K.S Ramaswamy

(Mr. K.S. Ramaswamy)
Sr. Manager (R&M),
NTPC/NCPS, Dadri,
Post – Vidyut Nagar,
Distt. - Gautam Budha Nagar
Pin – 201 008 (UP)

Satya Prakash

(Dr. Satya Prakash)
Professor,
Department of Metallurgical
and Material Engineering,
Indian Institute of Technology,
Roorkee, Roorkee - 247 667 (UA)

ACKNOWLEDGEMENT

I am extremely indebted to my thesis guide **Prof. Satya Prakash**, Department of Metallurgical and Materials Engineering, IIT Roorkee and **Mr. K.S. Ramaswamy**, NTPC/NCPS, Dadri, for their invaluable guidance at each level, constructive criticism and cheerful encouragement throughout this dissertation. It was a great pleasure, learning experience and satisfaction to work under their supervision.

I also express my gratitude to M.Tech-Coordinator for providing me help and facilities at IIT Roorkee.

No words are adequate to express my indebtness towards my beloved parents whose blessings have always shadowed me. These pages wouldn't be sufficient to mention their enormous support and encouragement. I express my abounding feeling to my brothers, sister and friends for their love to achieve this goal.

I am grateful to Mr. Amit Kumar Sahu, Mr. Rajeev Kumar Pandey, NTPC/NCPS for helping me in all aspects and providing valuable suggestions time to time.

Praveen Kumar Patel

November, 2003 **(PRAVEEN KUMAR PATEL)**

ABSTRACT

Composite materials with their well-known advantages have found widespread usage in various engineering applications. The metal matrix composites are, perhaps, the most important class among composites for automobile and aerospace applications because of their excellent mechanical and lubricating properties especially at high temperatures. During centrifugal casting of Aluminum melts containing suspended ceramic particles, segregation of the particles occurs either to the outer or to the inner periphery of the casting depending on their relative density compared to that of the melt. An one dimensional heat transfer model coupled with equations for force balance on particles is developed to predict the temperature distribution in the casting and mold regions, solidification time of the casting and particle distribution in the casting region. The model takes into consideration propagation of solid-liquid interface and movement of particles due to centrifugal acceleration which takes place either in opposite or in the same direction as the solidification front depending on the relative density difference between particles and melt. The solution of the model equations has been obtained by pure implicit finite difference technique with modified variable time step (MVTS) approach.

The effects of various parameters like particle size, mold rotational speed, relative density difference between melt and particle, etc. on segregation of particles and solidification time have been studied. It is noted that for a given set of operating conditions, the thickness of the particle rich region decreases with the increase in rotational speed of the mold, particle size, relative density difference between the particle and melt, and the melt superheat. When the interfacial heat transfer coefficient at the metal-mold interface is considered, the solidification time increases with decrease in heat transfer coefficient. Consequently, the thickness of the particle rich region decreases and hence, more intense particle segregation obtained in metal matrix.

CONTENTS

LIST OF TABLES

LIST OF FIGURES

LIST OF SYMBOLS

C	specific heat, $J\ kg^{-1}K^{-1}$
h_1	heat transfer coefficient at $r = 0$, $W\ m^{-2}\ K^{-1}$
h_2	heat transfer coefficient at $r = -r_i$, $W\ m^{-2}\ K^{-1}$
h_3	heat transfer coefficient at $r = -r_o$, $W\ m^{-2}\ K^{-1}$
h_4	heat transfer coefficient at $r = -r_g$, $W\ m^{-2}\ K^{-1}$
H	latent heat of solidification, $J\ kg^{-1}$
H_e	effective latent heat of solidification, $J\ kg^{-1}$
k	thermal conductivity, $W\ m^{-1}\ K^{-1}$
N	rotational speed of mold, *rpm*
R_e	*r*eynolds number
R_{ic}	position of casting inside from center, m
R_{ig}	position of graphite mold inside from center, m
R_{im}	position of steel mold inside from center, m
R_{oc}	position of casting outside from center, m
R_{og}	position of graphite mold outside from center, m
R_{om}	position of steel mold outside from center, m
R_p	particle radius, m
R_{pc}	critical size of the particle, m
$R_{s(t)}$	position of solid-liquid interface from center, m
$r, \bar{r}$	coordinate system
r_i	casting thickness, m
r_g	distance from casting outside to graphite mold outside, m
r_o	distance from casting outside to steel mold outside, m
$r_{0\,(t)}$	position of particle at time $t = 0$, m
$r_{i\,(t)}$	position of particle at time t, m
$r_i\,(t + \Delta t)$	position of particle at time $t + \Delta t$, m
$s(t)$	thickness of solid as a function of time, m

T	temperature, °C
T_f	solidification front temperature, °C
T_g	temperature of graphite mold, °C
T_I	initial cast-mold interface temperature, °C
T_L	liquidus temperature of base alloy, °C
T_{lc}	temperature of liquid region of composite, °C
T_M	initial temperature of the graphite and steel mold, °C
T_m	temperature of steel mold, °C
T_p	pouring temperature, °C
T_S	solidus temperature of base alloy, °C
T_{sc}	temperature of solid region of composite, °C
T_α	temperature related to position of steel mold ambient, °C
T_β	temperature related to position of cast inner surface ambient, °C
t	time, *sec*
$V_f\,(t + \Delta t)$	volume fraction of particle as function of $(t + \Delta t)$
V_r	Stokes velocity of the particle, m s^{-1}
V_s	volume of solid particles in each segment, m^3
Δt	time increment, *sec*
ρ_p, ρ_l	density of particle and liquid respectively, $kg\ m^{-3}$
α	thermal diffusivity, $m^2\ s^{-1}$
v	viscosity of base alloy, ,N s m^{-2}
v_c	apparent viscosity, N s m^{-2}
ω	angular velocity of mold, $rad\ s^{-1}$
δ_1	thickness of air gap between casting and graphite mold, m
δ_2	thickness of air gap between graphite mold and steel mold, m
γ	centrifugal acceleration, $rad\ s^{-2}$

Subscripts

g	graphite mold
ic	position of casting inner surface
ig	position of graphite mold inside
im	position of steel mold inside
L	liquid region of base metal
lc	liquid region of composite
m	steel mold
n	time step
oc	position of casting outer surface
og	position of graphite mold outside
om	position of steel mold outside
p	particle
S	solid region of base metal
sc	solid region of composite

Superscripts

P	present time stop
P + 1	previous time step

CHAPTER 1

INTRODUCTION

Composite materials have many advantages over conventional materials because of their superior performance in terms of their strength, stiffness, and other mechanical properties. The ceramic-matrix composites (CMCs), fiber reinforced polymers (FRPs), metal-matrix composites (MMCs), etc. are composites to name a few. Among these, the field of MMCs is developing at a rapid pace. Several groups of investigators all over the world, are engaged in research on various aspects of the MMCs with an overall objective of improving their performance [1].

During Centrifugal Casting processing of metal matrix composites segregation of particles occurs due to centrifugal force, either to the outer or to the inner part of the casting, depending on the relative density of the particles and the matrix. Various processing parameters, such as pouring temperature, solidification time, pouring pattern and thermal properties of the particles and matrix, will significantly influence the spatial arrangement of dispersed particles and the solidification microstructure which involved during the centrifugal casting of the composite.

To determine the solidification time and temperature distribution of the MMCs in centrifugal casting is difficult because ceramic particles move at a very high velocity. Hence for a realistic observation, the mathematical modeling concept comes into picture. The mathematical model which is formulated in this practice is essentially based on the heat transfer, particle segregation and solidification consideration. One of the important features of the present model is a more realistic representation of the variation of volume fraction of the particles across the thickness of the casting with time. Mathematical equations have been solved with the help of simple implicit finite difference techniques and using modified variable time steps.

CHAPTER 2

LITERATURE REVIEW

2.1 INTRODUCTION TO MMCs

Metal matrix composites (MMCs) are a class of advanced engineering materials in which a strong ceramic reinforcement is incorporated into a metal matrix to tailor its physical, mechanical and tribological properties for specific applications according to the design requirements. This creates new possibilities and challenges for the analyst and the designer, and makes accurate analysis, a necessity for sensitive applications. Because of these properties MMCs have played more important role in the areas of aerospace, automobile and other similar industries. The MMCs possess high temperature hardness, higher strength, higher elastic modulus and low sensitivity to temperature changes or thermal shock. The only drawback of the MMCs is that they possess less ductility than the matrix materials, which is overshadowed by the above-mentioned advantages [2,3].

The functional gradient composite (FGC) is a new type of composite, that has become attractive because of its multi-functional properties, including the reinforced ceramic particle properties, matrix metal properties, and their combined properties [4]. The FGCs are designed to have heat-resistant ceramics on their high temperature side and tough metal in their low temperature side, with a gradual compositional change. The main advantage of the FGC are the gradual change of properties such as coefficient of thermal conductivity and electrical conductivity, thermal stress etc. resulting from the gradient distribution of its structure and reinforced phases, which can avoid the destruction caused by the properties mismatch at high temperature.

2.2 METHODS OF PRODUCING MMCs

Ceramic reinforced MMCs can be prepared using several techniques. These are usually powder metallurgy and casting techniques such as squeeze casting, pressure infiltration, stirring casting, compo casting or rheocasting, centrifugal casting, etc. Powder metallurgy method is the major route of solid-state processing through which MMCs are produced. However, solid-state processing techniques require more time, costly equipments, and often these are cumbersome [5]. Compared to solid state methods, liquid-state processing (like casting techniques) characterize excellent advantages such as

- Lower production cost,
- Time consumed is less,
- Simple in operation,
- Secondary processes are minimized and,
- Intricate shapes can be produced.

Due to these advantages, liquid state processing techniques are becoming more popular. During liquid state processing of MMCs, it is necessary from the production and performance point of view, that there should be a perfect mixing of particles in the matrix melts. The mixing of ceramic reinforcing particles in the metal matrix depends on the method of producing MMCs as well as process variables involved. The main factors, which have a bearing on mixing behaviour, are:

- Physico-chemistry of wetting,
- Temperature and duration of preheat treatment of particles,
- Temperature of the matrix and holding time,
- Interface stability,
- Rate of addition of particles,

- Size of particles and,
- Percentage of particles etc.

During liquid-state processing rejection of ceramic particles by the melt is a common problem. This is because most of the liquid metals do not wet ceramic particles. This problem, however, can be overcome by employing techniques, which improve wetability. These include:

- Addition of alloying elements,
- Coating of reinforcing ceramic particles,
- Pre-heating of ceramic particles and,
- Stirring,

The fabrication of the FGCs has been accomplished via powder metallurgy techniques and deposition processes such as plasma spraying, physical vapour deposition (PVD), chemical vapour deposition (CVD), electro forming, and self-propagating high-temperature synthesis (SHS) [5]. Compositional gradient is achieved by varying the chemistry of the powders and reactive gases with time in PM, PVD and CVD processes, respectively. But these processes are hard to be applied in practical use due to complex techniques and high cost. This has lead to the development of an alternative technique. Centrifugal casting of MMCs is such an alternative technique to produce gradient composites very easily by controlling various process parameters according to the requirements.

2.3 CENTRIFUGAL CASTING OF MMCs

Centrifugal casting involves pouring a liquid metal into a rapidly rotating mould, which may be mounted either vertically or horizontally, and continuing the rotation until solidification is complete. The main advantages of this technique are good mould filling combined with good micro structural control, which usually give excellent mechanical properties. During centrifugal casting of MMCs segregation

of particles occurs due to centrifugal forces, either to the inner or to the outer part of the casting, depending on the relative densities of the particles and the melt, which results in particle reinforced FGCs [6-8]. The extent *of* segregation depends on various process parameters, such as pouring temperature, solidification time, thermo-physical properties of particles etc.

2.4 EARLIER WORKS ON THE CASTING OF THE MMCs/FGM

J.W. Gao et.al [5] have carried out numerical investigation of the solidification process during centrifugal casting of functionally graded materials (FGMs). They have developed a predictive model based on the multi phase modeling framework for FGM solidification by centrifugal casting. Using pure liquid water as the matrix and glass beads as the particle phase, uni-directional solidification, experiments were performed in a rectangular test cell to validate the multi phase model.

The model was used to investigate the solidification process in centrifugal casting of Al / SiC, FGMs in cylindrical mold. Three factors were identified to be responsible for creation of the particle concentration gradient: the geometrical nature of the particle flow in cylindrical mold, the angular velocity and the solidification rate which captures the desired gradient- it is the interruption of particle migration by the solidification front that creates gradients in the particle concentration.

Qingmin Liu et.al[9] have given a theoretical analysis to obtain gradient distribution of particles in centrifugal field by which the particle distribution gradient in the composite can be predicted. Particle movement in the liquid is described and gradient distribution of the particles in the composite is calculated in a centrifugal field during solidification.

Particle distribution in the composite produced by centrifugal casting are calculated under the conditions of

$d \geq \left| \frac{18\eta^2}{\Delta\rho\omega^2 r\rho_L} \right|^{1/3}$; where d = diameter of the particle, η = viscosity of the melt, ω = angular velocity, r = radial coordinate, ρ_L = density of the liquid metal, ρ_P = density of the particle and $\Delta\rho = \rho_P - \rho_L$.

The solidification rate R and angular velocity ω are assumed to be constant, and there is no interaction between particles and liquid metal. The particle volume fraction X_S in composite zone is derived as

$X_S = X_L^* \left(1 + \frac{V_r}{R}\right) e^{-A\omega^2 t}$; where X_L^* = particle volume fraction in melt added in mold, V_r = radial velocity,

In which $t = (r_m - r) / R$ and the distribution in melt is $X_L = X_L^* e^{-A\omega^2 t}$. The gradient of the particle distribution in the composite by centrifugal casting is calculated as

$$G = X_L^* x(2 + rx) e^{-x(r_m - r)}$$

Where $x = A\omega^2/R$ and $A = \frac{d^2\Delta\rho}{18\eta^2}$, r_m = internal radius of the mold;

G increases with increase of radius r for $\Delta\rho > 0$ and decreases with increase of radius r for $\Delta\rho < 0$. The factors which affect the gradient of particles distribution also include in solidification rate R, angular velocity ω particle diameter d, density difference $\Delta\rho$, and viscosity of melt η.

C.G.Kang et.al[10] have reported one dimensional heat transfer analysis during centrifugal casting of Aluminium alloy and copper based metal matrix composites containing Al_2O_3, SiC_p and graphite particles. In this model the particle segregation is calculated by varying the volume fraction during centrifugal casting. The numerical modeling of particle segregation during centrifugal casting of liquid metal containing suspended particle has been proposed. The volume fraction of graphite at the inner periphery, of the cylinder and near the graphite

free region is a strong function of mold rotational time. A maximum of 52 vol percent graphite could be concentrated at the inner periphery at a solidification time of 38 seconds. The temperature of the liquid region at the inner periphery of the composite cylinder depends on the speed of rotation, variation of reinforcement and base alloy.

2.5 MATHEMATICAL MODELING

A schematic representation of the model of centrifugal casting of a MMC is shown in Fig. 2.1. The heat is withdrawn from the liquid region of the casting, which is at temperature of T_{lc}, through the solidified composite region at temperature T_{sc}, to graphite mold at temperature T_g and subsequently through steel mold at temperature T_m to the surroundings. Heat is also radiated away from the inner surface of the casting. The dispersed particles in the liquid are at temperature T_{lc}. As the solidification proceeds by conduction of heat transfer through the composite to the graphite mold, the solid-liquid interface moves away from the graphite mold.

2.5.1 MODEL FORMULATION

The principal model equations are heat transfer equations for various regions comprising the process, and a force balance equation for the particulates to quantify the segregation of particles in the liquid region of the casting.

The model is based on the following assumptions:

1. The heat flow is purely one dimensional and perpendicular to the mold wall.
2. The mould is filled with liquid metal instantaneously.
3. Thermal properties of solid and liquid matrix melt are constant.
4. Heat transfer coefficient between casting and graphite mold decreases as the

solidification proceeds due to increase in air gap because of contraction of casting.

5. Natural convection and movement of particles due to buoyancy is neglected.
6. The interface position between solid and liquid regions is calculated by assuming it to be planar.
7. There is no thermal resistance between particles and liquid metal.
8. Particles are assumed to be spherical in shape.

2.5.1.1 HEAT CONDUCTION FORMULATION

The heat transfer processes in liquid melt, solidified casting region, graphite and steel mold regions are governed by one dimensional, unsteady state heat conduction equation written in cylindrical coordinates,

$$\frac{\partial T_i}{\partial t} = \alpha_i \left(\frac{\partial^2 T_i}{\partial r^2} + \frac{1}{r} \frac{\partial T_i}{\partial r} \right) \tag{2.1}$$

Where

$$\alpha_i = \frac{k_i}{\rho_i C_i} \tag{2.2}$$

and i = *lc, sc, g, m* for the liquid composite, solid composite, graphite and for steel mold regions, respectively.

The α_{lc} and α_{sc} are estimated by determining the volume fractions of the solid particulates in the liquid and solid composite regions, which vary with time due to movement of particles owing to the density difference between the liquid metal matrix and solid particulates. The thermal conductivity, density and specific heat of composite in either the liquid or solid regions are determined by the rule of mixtures described as follows as a function of volume fraction of particles $V_f(t)$ with various times *'t'*,

$$K_{sc} = (1 - V_f(t))\, k_s + V_f(t) k_p \tag{2.3}$$

$$K_{lc} = (1 - V_f(t))\, k_l + V_f(t) k_p \quad (2.4)$$

$$\rho_{sc} = (1 - V_f(t))\, \rho_s + V_f(t) \rho_p \quad (2.5)$$

$$\rho_{lc} = (1 - V_f(t))\, \rho_l + V_f(t)\, \rho_p \quad (2.6)$$

$$C_{sc} = (1 - V_f(t))\, C_s + V_f(t) C_p \quad (2.7)$$

$$C_{lc} = (1 - V_f(t)) C_l + V_f(t) C_p \quad (2.8)$$

Where, the volume fraction $V_f(t)$ depends on the viscosity of the alloy, particle size, mold rotational speed and the density difference between the particle and the molten metal.

The rate of solidification of the liquid composite is significantly dependent upon air gap formed at the casting-graphite mold interface due to the contraction of the casting as well as thermal expansion of the mold during solidification, and also to some extent the air gap at graphite mold-steel mold interface due to imperfect contact. It is assumed that the heat transfer coefficient between casting and graphite mold due to air gap varies as [11],

$$h_1 = h_i \left(\frac{h_f}{h_i} \right)^{\frac{s(t)}{r_i}} \quad (2.9)$$

Where, h_i is initial heat transfer coefficient, h_f is final heat transfer coefficient, s(t) is solidified thickness and r_i is total thickness of the casting.

Initial condition:

During centrifugal casting, before pouring the molten metal (which is at temperature T_p) into the mold, the mold is preheated to a certain temperature(T_M) to avoid the thermal damage to the mold. Therefore the initial temperature distribution (at time $t = 0$) in the casting and mold regions is considered as:

$$T_{lc} = T_p \quad (2.10)$$

$$T_g = T_m = T_M \quad (2.11)$$

As soon as the liquid metal comes in contact with the mold wall, the temperature of the metal-mold interface increases suddenly. The initial interface temperature can be approximated by considering the thermal energy conservation within the very thin layer of the metal and the mold in an adiabatic system [12]. The detailed description is presented in Appendix A.

Boundary conditions:

The boundary conditions in different regions of the casting and the mold are as follows :

1. At the inner surface of the casting, i.e., at r = R_{ic}

$$k_{lc}\frac{\partial T_{lc}}{\partial r} = h_2\left(T_{ci} - T_{\beta}\right) \tag{2.12}$$

2. At the outer surface of the casting, i.e., at r = R_{oc}

$$-k_{sc}\frac{\partial T_{sc}}{\partial r} = h_1\left(T_{co} - T_{gi}\right) \tag{2.13}$$

3. At the inner surface of the graphite mold, i.e., at r = R_{ig}

$$-k_{g}\frac{\partial T_{g}}{\partial r} = h_1\left(T_{co} - T_{gi}\right) \tag{2.14}$$

4. At the outer surface of the graphite mold, i.e., at r = R_{og}

$$-k_{g}\frac{\partial T_{g}}{\partial r} = h_4\left(T_{go} - T_{mi}\right) \tag{2.15}$$

5. At the inner surface of the steel mold, i.e., at r = R_{im}

$$-k_{m}\frac{\partial T_{m}}{\partial r} = h_4\left(T_{go} - T_{mi}\right) \tag{2.16}$$

6. At the outer surface of the steel mold, i.e., at r = R_{om}

$$-k_{m}\frac{\partial T_{m}}{\partial r} = h_3\left(T_{mo} - T_{\alpha}\right) \tag{2.17}$$

7. At solid-liquid interface, i.e., at r = $R_s(t)$

$$T_{sc} = T_{lc} = T_f \tag{2.18}$$

8. The energy balance at solid-liquid interface, i.e., at r = $R_s(t)$ is obtained *by* equating the rate of heat removed from the solid phase in the positive r direction to the sum of rate of heat supplied to the interface from the liquid phase in the positive r direction and rate of heat liberated at the interface during solidification, i.e.,

$$-k_{sc}\frac{\partial T_{sc}}{\partial r} = -k_{lc}\frac{\partial T_{lc}}{\partial r} + \rho_{sc} H \frac{\partial s(t)}{\partial t} \qquad (2.19)$$

2.5.1.2 PROBLEM FORMULATION IN TERMS OF DIMENSIONLESS VARIABLES

Since the problem does not permit an exact analytical solution, numerical solution techniques have been adopted, as these can provide results of assured accuracy. To facilitate solutions via a finite difference technique, it appears advantageous to work in a domain of unchanging size in which the grid can be fixed once and for all. This requires that the moving boundary be immobilized by the transformation of variables [10,13,14]. This also serves to introduce dimensionless variables. For this a new coordinate system with origin at the outer surface of the casting is defined which is schematically shown in Fig. 2.2. The thickness of the solidified front at a given time is represented by *s(t)*. The problem then is to find the time taken for the solid liquid interface to move from $\bar{r} = 0$ to $\bar{r} = r_i$.

The new space coordinates in solid and liquid regions are defined as

$$\xi = \frac{\bar{r}}{s(t)} = \frac{R_{oc} - r}{s(t)} \qquad (0 \le \bar{r} \le s(t)) \qquad (2.20)$$

$$\eta = \frac{\bar{r} - s(t)}{r_i - s(t)} = \frac{R_{oc} - r - s(t)}{r_i - s(t)} \qquad (s(t) \le \bar{r} \le r_i) \qquad (2.21)$$

so that $0 \le \xi \le 1$ and $0 \le \eta \le 1$ in the each region respectively for all the time. The following relations respectively for the solid and liquid regions facilitate the

transformation of the governing equations,

$$\frac{\partial}{\partial r} = \frac{-1}{s(t)}\frac{\partial}{\partial \xi}, \qquad \frac{\partial}{\partial r} = \frac{\partial}{\partial t} - \frac{\xi}{s(t)}\frac{ds(t)}{dt}\frac{\partial}{\partial \xi} \tag{2.22}$$

$$\frac{\partial}{\partial r} = \frac{-1}{r_i - s(t)}\frac{\partial}{\partial \eta}, \qquad \frac{\partial}{\partial t} = \frac{\partial}{\partial t} - \frac{(1-\eta)}{r_i - s(t)}\frac{ds(t)}{dt}\frac{\partial}{\partial \eta} \tag{2.23}$$

The additional terms in the transformation of terms in Eqs. (2.22) and (2.23), respectively, have an interesting physical interpretation. They represent convection associated with the immobilization of a moving boundary. An observer positioned on an immobilized moving boundary sees mass moving toward (or away) from him, and this mass is responsible for convection[15].

The transformation of governing equation (2.1) for solid region and the boundary conditions to the solid region, Eqs. (2.13) and (2.18), are written as follows, respectively,

$$\frac{\partial T_{sc}}{\partial t} = \frac{\alpha_{sc}}{s^2(t)}\frac{\partial^2 T_{sc}}{\partial \xi^2} + \left[\frac{\xi}{s(t)}\frac{ds(t)}{dt} - \frac{\alpha_{sc}}{R_{oc} - \xi s(t)}\frac{1}{s(t)}\right]\frac{\partial T_{sc}}{\partial \xi} \tag{2.24}$$

$$\text{at} \qquad \xi = 0 \quad \frac{k_{sc}}{s(t)}\frac{\partial T_{sc}}{\partial \xi^2} = h_1\left(T_{oc} - T_{ig}\right) \tag{2.25}$$

$$\textit{at} \qquad \xi = 1 \quad T_{lc} = T_{sc} = T_f \tag{2.26}$$

Similarly for the liquid region $0 \le \eta \le 1$ the Eq. (2.1) and the boundary conditions represented by Eqs. (2.18) and (2.12) are transformed, respectively, as

$$\frac{\partial T_{lc}}{\partial t} = \frac{1}{(r - s(t))}\left[(1-\eta)\frac{ds(t)}{dt} - \frac{\alpha_{lc}}{(R_{oc} - s(t)) - \eta(r_i - s(t))}\right]\frac{\partial T_{lc}}{\partial \eta} + \frac{\alpha_{lc}}{(r - s(t))^2}\frac{\partial^2 T_{lc}}{\partial \eta^2} \tag{2.27}$$

$$\text{at} \qquad \eta = 0 \quad T_{lc} = T_{sc} = T_f \tag{2.28}$$

$$\eta = 1 \quad \frac{-k_{lc}}{r_i - s(t)} \frac{\partial T_{lc}}{\partial \eta} = h_2 (T_{ic} - T_\beta) \tag{2.29}$$

The energy balance equation (2.19) at the solid-liquid interface can be rewritten as

$$\frac{\partial s(t)}{\partial t} = \frac{k_{sc}}{H\rho_{sc}} \left[\frac{1}{s(t)} \frac{\partial T_{sc}}{\partial \xi} - \frac{k_{lc}}{k_{sc}} \frac{1}{r_i - s(t)} \frac{\partial T_{lc}}{\partial \eta} \right] \tag{2.30}$$

The effective latent heat involved in solidification is also reduced because the ceramic particles contained in the composite melt are not involved in solidification process. The effective latent heat *(H_e)* is given by,

$$H_e = H\,(1 - V_f(t)) \tag{2.31}$$

Since there is no phase transformation in the two mold regions, Eq. (2.1) without transformation is used to calculate the graphite and steel mold temperatures.

2.5.1.3 FORCE BALANCE ON PARTICLES

Under a constant acceleration, when the fluid is under laminar flow, that is, the Reynolds number $R_e \leq 1$, the velocity of the spherical particle is deduced from Stokes law to be,

$$V_r = \frac{4R_p^2 \Delta\rho\omega^2 r}{18\upsilon} \tag{2.32}$$

Where R_p is radius of the particle, ω is angular velocity, r is particle position, ν is viscosity of the melt and $\Delta\rho = \rho_p - \rho_l$ density difference between the particle *(ρ_p)* and liquid metal *(ρ_l)*. The Reynolds number is given by,

$$R_e = \left| \frac{\rho_l V_r 2R_p}{\upsilon} \right| \tag{2.33}$$

During vertical centrifugal casting, a particle which is suspended in the liquid is subjected to a vertical acceleration due to gravity g and to a centrifugal acceleration $\gamma = \omega^2 r$. Generally γ is much greater than g which allows the vertical displacement of the particle to be ignored. Therefore the different forces on the particle are (i) centrifugal force due to the rotation, (ii) viscous force due to drag effect, and (iii) repulsive force due to movement of solid-liquid interface, which is shown in Fig. 2.3

The force balance equation on the particle due to centrifugal, viscous, and repulsive forces can be expressed as[16]

$$F_\omega - F_v - F_R = F_{net} \tag{2.34}$$

where F_{net} is net force on the particle, F_ω is force due to centrifugal acceleration, F_v is viscous force, and F_R is repulsive force. Since the repulsive force is significant only on those particles, which are in the vicinity of the solid-liquid interface, for the sake of simplicity from the calculation point of view, this term is neglected. The Eq. (2.34) can be rewritten as

$$\frac{4}{3}\pi R_p^3 (\rho_p - \rho_l)\omega^2 r - 6\pi\upsilon R_p \frac{dr}{dt} = \frac{4}{3}\pi R^3 \rho_p \frac{d^2 r}{dt^2} \tag{2.35}$$

Solution of Eq. (2.35) for a particle, moving at a constant velocity, which gives its position of the particle at any instant of time t as

$$r(t) = r_0(t) \exp\left[\frac{4\omega^2 (\rho_p - \rho_l) R_p^2 t}{18\upsilon} \right] \tag{2.36}$$

Where $r_o(t)$ is position of the particle at time t=0

Equations (2.32) and (2.36) are valid only when an isolated particle of radius,

$$R_p \le R_{pc} = \left| \left(\frac{9\upsilon^2}{4\Delta\rho\omega^2 r \rho_l} \right)^{\frac{1}{3}} \right| \tag{2.37}$$

is under movement in the liquid [17]. But several phenomena have to be considered when a liquid containing suspended particles is solidified in a mold rotating at high velocity.

- The interaction between the moving particles and the solidification front.
- The variation of viscosity of the liquid due to movement of particles.
- The interaction between the particles in the liquid.

In this regard, following assumptions are made

1. The motion of the particles is stopped by the liquidus front, i.e. the particles do not move in the mushy zone of the casting and they are not rejected by the solidification front.
2. Equations (2.32) and (2.36) are valid only for the motion of an isolated particle in a liquid. But for large volume fractions, interaction between particles occurs thus reducing their velocity. It is assumed that the reduction in velocity can be characterized by an increase of apparent viscosity of the liquid. The apparent viscosity can be represented as [18]

$$\upsilon_c = \upsilon\left[1 + 2.5V_f(t) + 10.05V_f^2(t)\right] \tag{2.38}$$

3. Furthermore it is assumed that segregation of particles can only occur up to a maximum volume fraction taken equal to 52%.

2.5.1.4 DETERMINATION OF VOLUME FRACTION

In order to determine the volume fraction variation in liquid metal matrix, the casting thickness is divided into *n* equal segments. Nodal points are considered at the extreme positions of each segment. The volume fraction of particulates in each segment is defined as the ratio of volume of particles to the total volume of the each segment and is given as

$$V_{fs} = \frac{V_s}{V_s + V_l} = \frac{1}{1 + \dfrac{\rho_s m_l}{\rho_l m_s}} \tag{2.39}$$

where V_s is the volume of reinforced particles, and V_l is the volume of the metal

matrix in each segment. Since the initial volume fraction of particles is known in each segment, the volumes and masses of the solid particles and matrix melt can be obtained using the following relationships,

$$V_s = V_{fs}\, V, \quad V_l = V - V_0 \tag{2.40}$$

$$m_s = V_s\, \rho_s, \quad m_l = V_l\, \rho_l \tag{2.41}$$

Where V is total volume of each segment, m_s is mass of solid in each segment, and m_l is total mass of liquid in each segment.

For simplicity, the particle positions are considered at the nodal points. The particles at different nodal points have different velocities, because the motion of each particle in the liquid melt is dependent on its position. The volume of particulates in between two consecutive nodal points always remains the same. The new particle positions can be obtained by Eq. (2.36). From the new particle positions, total volume of each segment of unit length can be obtained. The new volume fraction of particles in each segment at time, $t + \Delta t$ is obtained as follows:

$$\rho_l > \rho_p : V_f(t+\Delta t) = \frac{V_s}{\pi\left[r_i^2(t+\Delta t) - r_{i-1}^2(t+\Delta t)\right]} \tag{2.42}$$

$$\rho_p > \rho_l : V_f(t+\Delta t) = \frac{V_s}{\pi\left[r_{i+1}^2(t+\Delta t) - r_i^2(t+\Delta t)\right]} \tag{2.43}$$

CHAPTER 3

FORMULATION OF PROBLEM

During the centrifugal casting of particle reinforced MMCs, it is very difficult to determine the temperature distribution and solidification time by experimental techniques, as the mold rotates at a very high speed during solidification. Because of this, accurate data on solidification time and temperature distribution in the case of centrifugal casting of MMCs are not available. Therefore it is necessary to estimate the solidification time and the influence of other parameters on the solidification time in the case of centrifugal casting of metal matrix composite through indirect means. Analytical method involving heat and mass transfer analysis can be useful under such condition but this also becomes a complex problem.

Mathematical modeling of the casting process based on heat and mass transfer analysis can be a useful alternate methodology. Numerical solution of model equations using *"Finite Difference Technique" has* been attempted in the present study. The heat transfer coefficient between the cast-mold interface, mold speed, thermo-physical properties of particle, and initial temperatures of the melt and the mold are considered as basic parameters which have affect on solidification time and segregation of the particles in the MMCs.

Unlike the previous work of Kang and Rohatgi[10] in which the variation of the volume fraction is considered as a function of particle moving distance, the heat transfer coefficient between the metal-mold interface is assumed as constant, and the change in latent heat content due to presence of particles during solidification is neglected, in the present formulation the variations in the heat transfer coefficient and latent heat content are considered with appropriate relations. Also the variation of the volume fraction of the particles with time is

considered by ensuring the total mass of the particles in the casting is conserved for all the time.

The final attempt has been made to find out the effect of the various parameters like rotational speed, particle size, relative density difference, initial pouring temperature, heat transfer co-efficient etc. on the:

(i) Thickness of the particle rich region,

(ii) Solidification Time and

(iii) Temperature distribution within the casting as well as in the mold region.

CHAPTER 4

PROCEDURE FOR SOLVING MODEL EQUATIONS

The model equations have been solved numerically by using simple implicit finite difference technique. For this the "$\bar{r}-t$" *domain* is subdivided into small intervals of constant $\Delta\bar{r}$ in space and variable Δt in time as shown in Fig. 4.1. The variable time step approach is used to solve the problem. This approach requires that at each time level t_n the time step Δt_n is so chosen that the interface moves exactly a distance Δr during the time interval Δt, hence always stays on the node. Therefore, the problem is mainly concerned with the determination of the time step $\Delta t = t_{n+1} - t_n$ such that in the time interval from t_n to t_{n+1} the interface moves from the position $n\Delta\bar{r}$ to the next position $(n + 1)\ \Delta\bar{r}$.

4.1 FINITE DIFFERENCE APPROXIMATION

The differential equation and the boundary conditions for both the mold region and casting region can be discretized by using implicit method with the central difference scheme [19]. The thickness of each mold region is subdivided into n equal grids, but for casting region the total casting thickness is subdivided into n equal grids. The number of grids in the solid and liquid composite regions vary with time. It means that for the solid composite region the number of grids (n_i) goes on increasing as the solidification proceeds, and for the liquid composite region the number of grids $(n - n_i)$ decreases, but their sum always remains same as n

Equations (2.1), (2.24), and (2.27) are solved with boundary conditions Eqs. (2.14) through (2.17), (2.25), (2.26), and (2.29) using implicit finite difference scheme. The resultant discretized equations are arranged in tridiagnol matrix form and the solution of these equations can be obtained by using Thomas Algorithm (TDMA) which will give temperature distribution in both casting and mold regions for a particular time step Δt_n. The detailed description is presented in Appendix B.

4.2 DETERMINATION OF TIME STEPS

During the solidification the interface moves from the position $n\Delta\bar{r}$ to the position $(n + 1)\,\Delta\bar{r}$ within a time interval of $\Delta t_i = t_{i+1} - t_i$ (shown in Fig. 4.2). Using modified variable time step (MVTS) method, the actual value of Δt_i is obtained by iteration as follows [20],

1. An initial guess value for the time step Δt_i chosen as $\Delta t_i = \Delta t_i^{(0)}$
2. Using $\Delta t_i^{(0)}$, first estimate for the nodal temperatures is obtained by solving the finite difference equations for the mold and casting regions.
3. First estimate for the time step $\Delta t_i^{(1)}$ is obtained by using estimates
   $\left[T_{lc_i}^{p+1}\right]^{(0)}$ and $\left[T_{lc_{i+2}}^{p+1}\right]^{(0)}$
4. Using $\Delta t_i^{(1)}$ repeat the steps (2) and (3) to obtain $\Delta t_i^{(2)}$
5. Iteration is carried out until the difference between the two consecutive time steps satisfies a specified convergence criterion.
6. To obtain Δt_{i+1} assume $\Delta t_{i+1}^{(0)} = \Delta t_i$ and repeat the steps from (2) to (5).
7. Repeat steps from (2) to (6) till the solid-liquid interface reaches the inner surface of the casting.

4.3 SEGREGATION OF PARTICLES

During centrifugal casting, segregation of particles takes place in the liquid composite due to the movement of particles resulting from difference in densities of the particles and the melt, and also due to centrifugal acceleration. By solving the Eqs. (2.42) and (2.43) through Eq. (2.36) and Eq. (2.38), the thickness of the particle rich region can be estimated for various rotational speeds of the mold at various times. The particle movement is neglected in the mushy zone of the casting, which is characterized by the temperature region ($T_s \leq T \leq T_L$), because in this zone the viscosity, ν_c, sharply increases.

CHAPTER 5

RESULTS AND DISCUSSION

The model equations are solved to evaluate (i) thickness of the particle rich region, (ii) solidification time, and (iii) temperature distribution within the casting as well as in the mold regions, for various operating conditions. The variables examined are (i) rotational speed of the mold, (ii) heat transfer coefficient between cast-mold interface, (iii) initial temperatures of liquid metal and mold, and (iv) thermo physical properties of particles. Thermo physical properties of matrix metal, reinforcement particles, and graphite and steel molds used in the simulation are given in Table 4.1 [21,22]. Various design and operating parameters, like geometric constants for the casting and the mold, the heat transfer coefficients at different regions of the casting and the mold, and initial temperatures of the mold and metal used in simulation are tabulated in Table 4.2 [10,22]. The cooling conditions at the inner surface of the casting and at the outer surface of the steel mold are defined in terms of heat transfer coefficients h_2, h_3 respectively and the heat transfer due to the air gap at the metal-mold interface is characterized by the heat transfer coefficient h_1. Since the actual values of h_1 are not known, computations have been carried for a wide range of values of this coefficient 1000 to *5000* $Wm^{-2}K^{-1}$. The results of simulation are presented in the following sections:

Table 5.1: Thermo physical properties of matrix metal, reinforcement particles, and mold materials.

Themophysical properties	Aluminium (A356)	Al_2O_3	SiC	Graphite	Carbon Steel Mold	Graphite Mold
$K(Wm^{-1}K^{-1})$	159	24	24	38	57.8	38
$\rho(kgm^{-3})$	2685	4000	3200	1900	7800	1900
$C(Jkg^{-1}K^{-1})$	963	600	690	710	481	710
$T_S(^0C)$	555	-	-	-	-	-
$T_L(^0C)$	615	-	-	-	-	-
$T_f(^0C)$	555	-	-	-	-	-
$H(KJkg^{-1})$	389	-	-	-	-	-
$\upsilon(Nsm^{-2})$	0.002	-	-	-	-	-

Table 5.2: Design & operating parameters used in simulation

Outer dia of steel mold, D_{om} *(mm)*	215.0
Outer dia of graphite mold, D_{og} *(mm)*	150.0
Outer dia of casting, D_{oc} *(mm)*	100.0
Inner dia of casting, D_{ic} *(mm)*	80.8
Heat transfer coefficient between the mold-metal interface, h_1 *($W m^{-2} K^{-1}$)*	1000 to 5000
Heat transfer coefficient at the inner surface of casting, h_2 *($W m^{-2} K^{-1}$)*	8.4
Heat transfer coefficient at the outer surface of steel mold, h_3 *($W m^{-2} K^{-1}$)*	8.4
Heat transfer coefficient between the graphite-steel mold interface, h_4 *($W m^{-2} K^{-1}$)*	10000
Initial pouring temperature of liquid metal, T_p *(°C)*	730
Initial mold temperature, T_M *(°C)*	250
Speed of rotation, *N (rpm)*	1000
Particle size, R_p *(μ,m)*	2
Initial heat transfer coefficient due to air-gap at the metal-mold interface, h_i *($W m^{-2} K^{-1}$)*	1000
Ratio of initial to final heat transfer coefficient, $\frac{h_i}{h_f}$	10

5.1 PARTICLE SEGREGATION CALCULATIONS

For various sets of operating conditions, the thickness of particle rich region has been calculated. Typical results of these calculations are presented in the form of (i) volume fraction and (ii) thickness of particle rich region for the entire region of the casting in Figs. (5.1) through (5.6). The main parameters, which influence the displacement velocity of the particles, are centrifugal acceleration, size of the particle, and relative density difference between the particle and the melt.

5.1.1 EFFECT OF ROTATIONAL SPEED OF CASTING

Figure. 5.1 shows the effect of speed of rotation of casting on the thickness of particle rich region, for three different values of rotational speeds, namely 1000, 1250, and 1500 rpm. Figure. 5.1(a) is for the case where the reinforcement particles are heavier than the matrix melt, while the Fig. 5.1(b) represents the case when the matrix melt is heavier than the reinforcement particles. From this figure, it is evident that with the increase in speed of rotation, the thickness of the particle rich region decreases. This is due to the fact that as the speed of rotation increases the centrifugal acceleration increases which causes increase in centrifugal force on the particles. Depending upon the relative density difference between the particles and the matrix melt, and whether it is positive or negative, the particulates move with greater velocity towards the outer or inner periphery of the casting. The thickness of the Al_2O_3 rich region varies from 0.008 to 0.0053 m, while that of the graphite-rich region thickness varies from 0.0086 to 0.007 m as the speed of rotation increases from 1000 to 1500 rpm, after 10 seconds from the start of solidification, as shown in Fig. 5.1.

5.1.2 EFFECT OF PARTICLE SIZE

Figure. 5.2 shows the effect of particle size R_p on the thickness of the particle rich region, for three different values of R_p, namely 1, 2, and 3 μm. From

this figure, it is evident that the thickness of the particle rich region decreases with increase in particle size leading to more intense segregation in both cases, i.e. (i) when $\rho_p > \rho_l$, and (ii) when $\rho_p < \rho_l$. While in the former case particles are segregated towards the outer periphery, in the latter case the segregation is towards the inner periphery.

During the particle motion in the liquid melt, the centrifugal and the viscous force on the particle will act opposite to each other. With increase in particle size, both the centrifugal and viscous forces increase, but the increase in centrifugal force is more than that in viscous force. Hence, larger particles move rapidly towards the outer or inner periphery of the casting depending upon the relative density difference between the particles and the liquid melt. The thickness of the particle rich region for $Al - Al_2O_3$ and $Al - Gr$ composites varies from 0.0095 to 0.0053 m, and from 0.0096 to 0.007 m respectively, as the particle size increases from 1 to 3 μm after 10 seconds of solidification time, as is shown in Fig. 5.2

5.1.3 EFFECT OF RELATIVE DENSITY DIFFERENCE BETWEEN PARTICLE AND MELT

Figure. 5.3 shows the effect of relative density difference between particles and melt, $(\rho_p - \rho_l)$, on the thickness of the particle rich region. The thickness of the particle rich region for SiC particles is more than that for the Al_2O_3 particles. With increase in relative density difference between particles and liquid metal matrix, the net centrifugal force on the particle increases which in turn, results in moving the particle to a farther distance. This leads to more intense particle segregation towards the outer periphery of the casting for the case $\rho_p > \rho_l$. As the particulate density increases from 3200 to 4000 $kg\ m^{-3}$, the thickness of the particle rich region decreases from 0.0088 to 0.0068 m after a period of 10 seconds from the start of solidification as is shown in Fig. 5.3. The speed of rotation in this simulation has been maintained at 1250 rpm.

5.1.4 EFFECT OF INITIAL POURING TEMPERATURE

Figure. 5.4 shows the effect of initial pouring temperature of the metal on the particle segregation, for three different values of T_p , namely 650, 730 and 800 °C for three particle sizes, namely 1, 2, and 3 *μm.* The heat transfer coefficient h_i in this simulation is taken to be as 5000 $W\,m^{-2}\,K^{-1}$. From the Fig. 5.4 it is evident that, with the increase in initial pouring temperature (T_p), the thickness of the particle rich region decreases, or in other words, the thickness of the particle free region increases for all three particle sizes considered. Higher initial pouring temperature essentially means that more heat is to be removed from the MMC melt before the solidification begins. Hence, it takes long time for the MMC melt to solidify. During this extra time period, the reinforcement particles are able to segregate more.

5.1.5 EFFECT OF INITIAL MOLD TEMPERATURE

Figure. 5.5 shows the effect of initial mold temperature (T_M) on the thickness of the particle free region for three different values of T_M namely 200, 250, and *300°C* for three particle sizes, viz 1, 2, and 3 *μm.*

For this simulation also the heat transfer coefficient between the metal-mold interface is taken to be 5000 $W\,m^{-2}K^{-1}$. It is observed that, with the increase in initial mold temperature, the thickness of the particle free region increases as in the previous case. In this case also with increase in mold temperature, solidification time increases because of the reduced heat transfer between the melt and the mold owing to the reduced thermal gradient between two. This again leads to more intense segregation. From the comparison of Figs. 5.4 and 5.5 it is evident that the effect of initial mold temperature on intensity of segregation is much more as compared to the effect of initial pouring temperature.

5.1.6 EFFECT OF HEAT TRANSFER COEFFICIENT AT THE MOLD-METAL INTERFACE

Figure 5.6 shows the effect of the heat transfer coefficient between the mold-metal interface (h_1) on the thickness of the particle rich region. From the figure it is evident that the heat transfer coefficient is a key parameter for particle segregation. It is known that the rate of heat transfer is directly proportional to the heat transfer coefficient between the metal-mold interface. With reduction in heat transfer coefficient, the heat removal rate decreases. Hence, the total heat required for solidification of composite casting increases, resulting in more segregation of the particles. Accordingly a reduction in the thickness of the particle rich region is observed in Fig. 5.6

5.1.7 EFFECT OF SOLIDIFICATION TIME

Figures. 5.7 and 5.8 show the variation of volume fraction of particulates as a function of time for three different particle sizes, namely, I, 2, and 3 μm. The heat transfer coefficient between the metal-mold interface in these two simulations are taken to be 2000 and 5000 $W\ m^{-2}K^{-1}$ respectively. From these figures it is evident that, with the increase in solidification time, more time is allowed for the particles to move in the liquid melt. Thus results in more intense segregation of particulates. It is also observed that with increase in particle size or decrease in heat transfer coefficient, there is a reduction in the thickness of particulate rich region as discussed earlier (Figs. 5.2 and 5.6). From Figs. 5.7 and 5.8, it is observed that the heat transfer coefficient at the metal-mold interface, h_1, is one of the important, parameters along with the particle size, which control the intensity of segregation. With increase in h_1, the heat removal rate increases. Hence, the total time required for solidification decreases, resulting in lesser segregation of the particles. The final thickness of the particle region for $Al\text{-}Al_2O_3$ varies from 0.007 to 0.002 m and 0.0078 to 0.0022 m for the values of heat transfer coefficient 2000 and 5000 $Wm^{-2}K^{-1}$, respectively, as the particle size increases from 1 to 3 μm. By increasing particle size from 1 to 3 μm almost all the particles are segregated towards the outer periphery of the casting.

5.1.8 EFFECT OF PARTICULATE VOLUME FRACTION

Figure 5.9 shows the effect of initial volume fraction of the particulates on the final distribution of the volume fraction of particulates and also on the thickness of the particulate rich region of the casting. From the figure it is evident that with increasing initial volume fraction of solid particulates, the final thickness of the particulate rich region increases. With increasing initial volume fraction of particulates viscosity of the liquid composite increases, there by reduces the motion of the particles. This results in more particle rich region.

5.2 SOLIDIFICATION TIME CALCULATION

For various sets of operating conditions, the times required for complete solidification of the casting have been calculated. Typical results of these calculations are presented in the form of (i) solidified thickness of the shell, and (ii) total solidification time, in figs. 5.10 through (5.14). The main parameters, which have effect on solidification rate, are the pouring temperature, the mold temperature, and the heat transfer coefficient at the metal-mold interface.

5.2.1 EFFECT OF INITIAL POURING TEMPERATURE

Figure 5.10 shows the development of the solid shell thickness as a function of solidification time for three different initial pouring temperatures, namely, 650, 730, and 800 °C. The time for complete solidification of the casting is the time when the shell thickness becomes 0.01 m (the casting thickness). It is evident that the time for complete solidification increases with increase of initial pouring temperature of the molten metal. This is due to fact that with increase in T_p , total heat content increases and more time is required to withdraw this excess heat. Figure 5.11 shows the variation of total solidification time as a function of initial pouring temperature for Al_2O_3 particles of three different sizes, viz, 1, 2, and 3 μm. It is seen that total solidification time substantially increases with increasing particle size. From the earlier discussion on effect of particle size on particle segregation (Fig. 5.2) it is evident that more intense segregation takes place with increasing particle size. Since Al_2O_3 particles are heat resistant

materials, with the increase in volume fraction near the outer periphery of the casting the thermal diffusivity substantially decreases in that region. This results in decrease in rate of heat withdrawal necessitating longer duration for solidification of the casting.

5.2.2 EFFECT OF INITIAL MOLD TEMPERATURE

Figure 5.12 is a plot of solidified shell thickness as a function of solidification time for four different initial mold temperatures, namely, 200, 250, 300, and 350 °C. From this figure it is evident that the time required for complete solidification of the casting increases with increase in initial mold temperature. As the initial mold temperature increases, the temperature gradient between the composite and the mold decreases which in turn reduces the heat transfer rate. This results in longer time for complete solidification of the casting. From Fig. 5.13 it is further observed that the total solidification time increases with the increase in particle size as in the case of Fig. 5.11.

5.2.3 EFFECT OF HEAT TRANSFER COEFFICIENT AT THE MOLD-METAL INTERFACE

Figure 5.14 shows the effect of heat transfer coefficient at the metal-mold interface (h_1) on solidification rate. In this figure the variation of the solidified shell thickness as a function of solidification time is plotted for three different values of h_1 namely, 1000, 2000, and 5000 $W\ m^{-2}\ K^{-1}$. It may be noted that h_1 itself changes with time according to the Eq. (2.9). It is observed that, as the value of h_1 decreases the interface offers more resistance to heat transfer from casting side to the mold. This leads to requirement of more time for complete solidification, as shown in Fig. 5.14.

As the solidification proceeds the thickness of the air-gap formed between the metal-mold interface goes on increasing due to contraction of the casting and also due to thermal expansion of the mold. This results in reduction in heat transfer coefficient between the metal-mold interface with time. Thus the rate of solidification decreases as the solidification front progresses from outer to the inner periphery of the casting, which is evident from Figs. 5.10, 5.12 and 5.14.

5.2.4 EFFECT OF PARTICULATE VOLUME FRACTION

Figure. 5.15 shows the variation of total solidification time as a function of the volume fraction of reinforcement particulates. As the initial volume fraction of particulates increases the effective thermal diffusivity of composite reduces. This results in longer time duration for complete solidification of the casting.

5.3 TEMPERATURE PROFILES IN THE CASTING AND MOLD REGIONS

The temperature profiles in the casting as well as mold regions have been calculated solving the energy balance equations along with the appropriate boundary conditions given in Appendix B. Figure 5.16 is a plot of temperature profiles at the outer and inner surfaces of the graphite mold region at rotational speed of 1000 rpm for three different values of h_1, namely 1000, 2000, and 5000 $W\,m^{-2}K^{-1}$. Higher interfacial heat transfer coefficient results in higher temperature both at the inner as well as outer surfaces of the graphite mold. This is because the higher heat transfer coefficient signifies better thermal contact between the casting and mold. From the figure it is evident that with the decrease in h_1 there is local cooling effect at the inner surface of the mold. Figure 5.17 shows the variation of temperature at the outer surface of the casting for different values of h_1. It is seen that with decreasing h_1, there is a local heating effect at the outer surface of the casting. It is further noted that with decreasing h_1 the local heating begins at the early stages of the solidification.

Due to the reduction in heat transfer coefficient between the metal-mold interface with time, the rate of heat transfer from the casting to the mold goes on decreasing. Since the interface is unable to discharge the amount of heat supplied to it from the liquid region of the casting through the solidified shell, there is a local heating effect on the casting side near the outer periphery. Similarly the rate at which the heat is been supplied from the metal-mold interface to the mold is less than the rate at which the heat is withdrawn from the

mold wall to the ambient. This causes local cooling at the inner periphery of the mold, as shown in Figs. 5.16 and 5.17.

5.4 DISCUSSION

The salient feature of the present formulation is a more realistic representation of the variation of the volume fraction of the particles due to particle movement in the liquid composite region. Unlike the previous work of Kang and Rohatgi[10] in which the variation of the volume fraction is considered as a function of moving distance only and the effect of presence of particle on the latent heat of solidification is neglected, the variation of volume fraction in the present formulation is estimated ensuring that the total mass of particles in the casting is conserved at all times and the latent heat of composite melt is modified depending upon the volume fraction of the liquid metal matrix in the melt.

The earlier works of J.W. Gao and C.Y. Wang[5] and Kang and Rohatgi[10] showed the effect of various parameters on the particle segregation, solidification time and temperature profiles in the casting and mold region. The present model is not only matches with theirs results but may also predict more efficiently and can be compared.

1) **Effect of rotational speed :-** They have given that with the increase in rotational speed, the particle rich region decreases. This model also indicates the same result as can be seen in fig 5.1(a) and 5.1 (b).
2) **Effect of particle size :-** J.W. Gao and C.Y. Wang[5] predicted that the larger particle size settle faster than the smaller particle. For larger particle, larger is the particle free region and for smaller particle, smaller is the particle free region. Our result also predicts that the thickness of the particle rich region decreases with increase in particle size as shown in fig 5.2.
3) **Effect of relative density difference :-** Kang and Rohatgi[10] shows that higher the density difference between the base alloy and reinforcement, the more is the particle segregation. The present model shows that with

increase in density difference, particle segregation at the outer periphery of the casting will increase as can seen be from fig 5.3.

4) **Effect of Initial Mold Temperature :-** Kang and Rohatgi[10] have reported that the solidification time increases with the increase in initial mold temperature. Our model also predicts the similar result as shown in fig 5.12 and also indicate that with increase in initial mold temperature, the thickness of the particle free region will increase as can be inferred from fig 5.5.
5) **Effect of Heat transfer coefficient :-** J.W. Gao and C.Y. Wang[5] have found that a lower cooling rate will allow the particles to settle and hence form a longer particle free region. Our model also arrives at same conclusion [fig 5.6] Kang and Rohangi [10] had reported that the higher the value of h_1, the lower the temperature distribution between the graphite mold and the casting region. Our result also indicates same trends as can be seen in fig 5.17.
6) **Effect of Particle volume fraction :-** J.W. Goa and C.Y. Wang [5] had repated that the thickness of the particle free zone decreases with increasing initial particle volume fraction. The present model gives that with increasing initial volume fraction of solid particulates, the final thickness of the particulate region increases, as shown in fig 5.9.

The force balance on the particles and energy balance equations are nonlinear and mutually coupled. Solution of such partial differential equations in their original form is often difficult because of the associated problem of convergence and also the boundary is moving with time. It is a advantage to work in the domain of unchanging size in which the grid is fixed once and for all. One way to get around this problem is to transform the governing differential equations and the associated boundary conditions into their equivalent dimensionless forms. In the dimensionless form the system of equations becomes scale free.

Formulation of the model is based on assumptions, some of which may only be partially valid. For instance, the assumption of interface between the solid and liquid region to be planar is an approximation. Strictly speaking the solidification front can be planar, cellular or dendrite depending upon the rate of solidification. It is very difficult to predict the either cellular or dendrite morphology of the solidification front, hence the assumption of planar solidification front is made.

The assumption of negligible thermal resistance between the particles and melt can also be questioned. In actual practice there may be some solubility of solid particulates in the liquid matrix, or some chemical reaction between the two. In both cases there may be a heat reaction associated with the phenomena taking place at the surface of the particle. This heat may appear as a heat source at the particle melt interface. Further, a chemical reaction at the surface may result in formation of a product layer which offers thermal resistance to the heat flow, resulting in distortion of the temperature field around the particle. This may, in any case, happen also due to the different thermal conductivities of the particle and melt.

The assumption of temperature invariant thermal properties is just for convenience. If the reliable expressions for thermal properties as function of temperature are available, these can be easily incorporated in the model equations.

CHAPTER 6

CONCLUSIONS

A mathematical model based on particle segregation, heat transfer and solidification considerations have been formulated to simulate the centrifugal casting process of Aluminum matrix composites. Model equations include energy balance for various zones and force balance on particles to find the particle, position and volume fraction. To make the model more general and also to work in a domain of unchanging size in which the grid can be fixed once and for all, the heat transfer equations and boundary conditions for the casting region are written in terms of dimensionless variables. Variation of the particle volume fraction in the casting region is considered by assuming that the total volume of particulates in each segment remains the same at all times, but the total volume of each segment itself changes with time and the total mass of particles in the casting is conserved at all times.

For the solution of the model equations an implicit finite difference scheme is employed, in which for the first order diffusive terms central difference scheme is adopted. The resulting equations are arranged in a tridiagonal matrix form and are solved by using Thomas Algorithm [20]. In order to find the solidification time for each segment, an iterative procedure, called modified variable time step (MVTS)[21] approach has been used. The model equation has been solved in one dimension in radial coordinate system and for unit length of the cylinder.
Based on simulation results, following conclusions are drawn:

1. For a given set of operating conditions, the thickness of the particle rich region decreases with the increase of (i) speed of rotation of the mold, (ii) particle size, and (iii) relative density difference between the particle and melt.

2. When an interfacial heat transfer coefficient at the metal-mold interface is considered, both the solidification time as well as the thickness of the

particle rich region decreases with the decrease in heat transfer coefficient.

3. A higher superheat of melt requires more time to for the metal to solidify, which results in reduction of the thickness of the particle rich region.

4. The initial temperature of the mold (preheating temperature) has a significant influence on the solidification time depending upon the relative value of the interfacial heat transfer coefficient.

5. For a given set of operating parameters, the solidification time increases with the increase in particle size. This is due to lowering of the thermal diffusivity of the composite due to increase in the volume fraction of the insulating reinforcement particles.

6. As the heat transfer coefficient at the graphite mold-casting interface decreases, there is a local heating effect in the outer region of the casting and a local cooling effect at the inner surface of the graphite mold.

This proposed model predicts very well the effect of various parameters on the particle segregation, solidification time of the mold and temperature profiles in the casting and mold regions. This model can also be used for regulating the different parameters which can effect on the centrifugal casting of metal matrix composites with the help of this model one can obtain the desired mechanical and tribological properties by varying the speed of rotation, particle size, relative density difference, initial pouring temperature, initial mold temperature heat transfer coefficient etc. The model developed in this study may also be used as a tool to develop prototype for the desired properties of cast under certain casting conditions.

6.1 SCOPE FOR FUTURE WORK

Any model developed is based on the certain assumption. These may vary and if certain other variables incorporated then problem becomes more realistic. The future work may incorporate:

(1) Interaction of particles with the solidification front i.e. particle pushing and particle clustering be incorporated into the model.

(2) Consideration of two dimensional heat flow.

(3) The fact that mold is filled slowly should also be considered.

(4) Consider the thermal resistance between particles and liquid metal.

(5) The variation of viscosity may be considered because there is interaction of particles.

REFERENCES

1. Taya M. and Arsenault R.J., "*Metal Matrix Composites Thermo Mechanical Behaviour*", Pergaman Press, New York, (1989), pp 1-8.

2. Macdanels D. L., "*Analysis of Stress-Strain, Fracture, and Ductility Behaviour of Aluminum Matrix Composites containing Discontinuous Silicon Carbide Reinforcement*", Metall. Trans.A, (1985), vol.16A, pp. 1105-1115.

3. Little J. A., McCracken D. and Simms N., *"High-Temperature Oxidation of a Particulate SiC - Aluminum Metal Matrix Composites"*, J. Mater. Sci. Lett., (1988), vol.7, p. 1037.

4. Clyne T.W. and Withers P.J., "*An Introduction to Metal Matrix Composites*", Cambridge University Press, (1993), pp 1-7.

5. Gao, J.W. and Wang C.Y., "Modeling the solidification fo fuctionally graded materials by centrifugal casting", Materials Science and Engg., A-292 (2000), pp 207-215

6. Nath D. and *Rohatgi* P.K., *"Segregation of Mica Particles in Centrifugal and Static Castings of Al-Mica Composites"*, Composites, (1981), pp. 124-128.

7. Krishnan B.P., Shetty H.R. and Rohatgi P.K., "*Centrifugally Cast Graphitic Aluminum with Segregated Graphite Particles*", AFS Trans., (1976), vol.76, pp. 73-80.

8. Lajoye L. and Suery M., *"Centrifugal Casting of Aluminum Alloy Matrix Composites"*, Solidification Processing 87, Sheffield 21-24 Sept., (1987), pp. 443-446.

9. Qingmin Liu, Yuning Jiao, Yuansheng Yang and Zhuangqi Hu, *"Theoretical Analysis of the Particle Gradient Distribution in Centrifugal Field During Solidification"*, Metall. Trans. B, (1996), vol.27B, pp. 1025-1029.

10. Kang C.G. and Rohatgi P.K., *"Transient Thermal Analysis of Solidification in a Centrifugal Casting for Composite Materials containing Particle Segregation"*, Metal. Trans. B, (1996), vol.27B, pp. 277-285.

11. Lajoye L. and Suery M., *"Modeling of Particle Segregation during Centrifugal Casting of Al-Matrix Composites"*, Proc. Intl. Symp. on advances in cast rein- forced metal composites, Publ. ASM Intl., (1988), pp. 15-20.

12. Ebisu Y., *"Computer Simulations on the Macro structures in Centrifugal Casting,* AFS Trans., (1977), vol.77, no.35, pp. 643-654.

13. Ramachandran N., Jaluria Y. and Gupta J.P., *"Thermal and Fluid Flow Characteristics in One Dimensional Solidification* ", Letters in Heat and Mass Transfer, (1981), vol.8, pp. 69-77.

14. Saitoh T., *"Numerical Method for Multi-Dimensional Freezing Problems in Arbitrary Domains"*, Trans. ASME, J. of Heat Transfer, (1978), vol. 100, May, pp.294-299.

15. Sparrow E.M., Ramadhyani S., Patankar S.Y., *"Effect of Sub-cooling on Cylindrical Melting"*, ASME, Journal of Heat Transfer, (1978), vol.100, no.2, pp. 395-402.

16. Szekely J., *"Fluid Flow Phenomena in Metal Processing"*, Academic Press, New York, NY, (1979), pp. 255-263.

17. Stefanescu D. M., Moitra A., Kacar A. S., and B. K. Dhindaw, *"The Influence of Buoyant Forces and Volume-Fraction of Particles on the Particle Pushing/ Entrapment Transition During Directional Solidification of Al-SiC and Al-Graphite Composites"*, Metall. Trans. A, (1990), vol. 21A, pp. 231-239.

18. Sasikumar R. and Pai B.C.," *Redistribution of Second-Phase Particles in Melt during Solidification: Computer Model"*, Solidification Processing 87, Sheffield 21-24 Sept., (1987), pp. 443-446.

19. Gupta Santosh K., "*Numerical methods for Engineers", New Age Intl. (P) Ltd., New Delhi, (1998), pp. 239-242.*

20. Gupta R.S. and Kumar Dhirendra, *"Variable Time Step Methods for One Dimensional Stefan Problem with Mixed Boundary Condition",* Int. J. Heat and Mass Transfer, (1981), vol. 24, pp. 251-259.

21. ASM Speciality Handbook, *"Aluminum and Aluminium alloys",* ASM International, (1994), p. 718.

22. Metals Handbook, 10th ed., ASM International, Materials Park, OH, (1992), vol.2, p. 164.

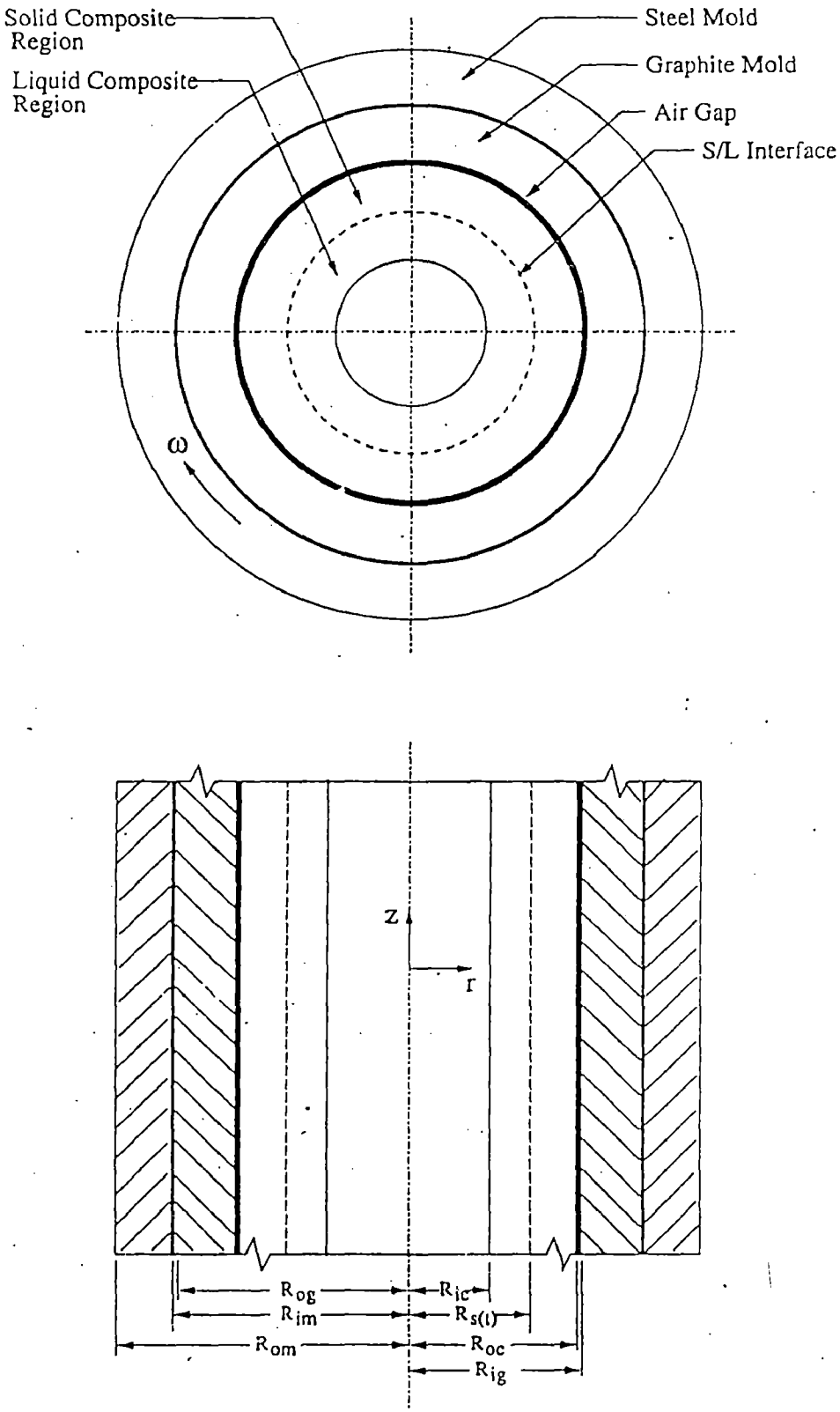

Fig (2.1) Schematic representation of the complete system of centrifugally cast MMC's with particle segregation and solidification interface.

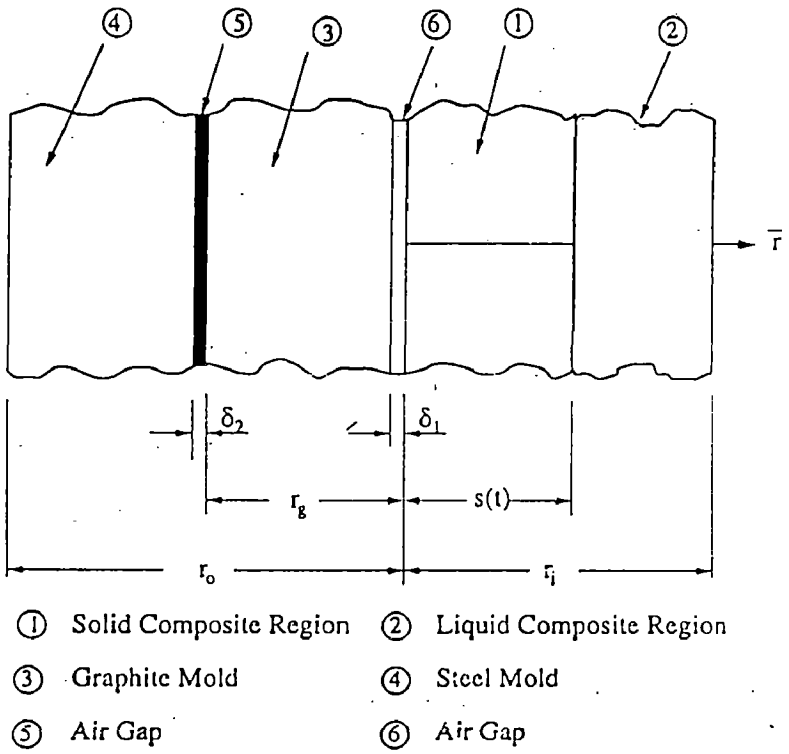

Fig (2.2) One dimensional model to find the temperature distribution and position of the solid-liquid interface

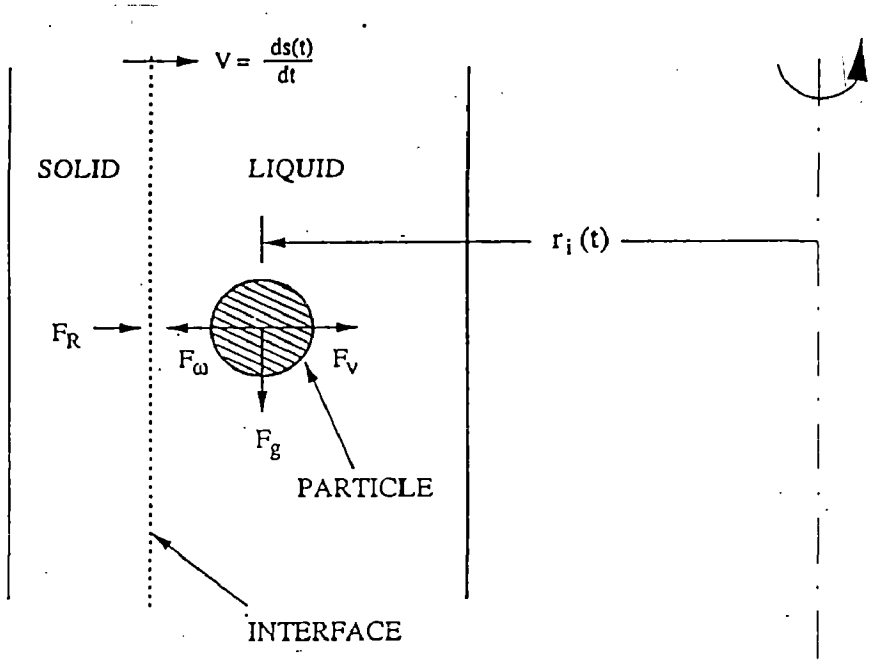

Fig (2.3) Schematic representation of various forces on the moving particle in the liquid melt

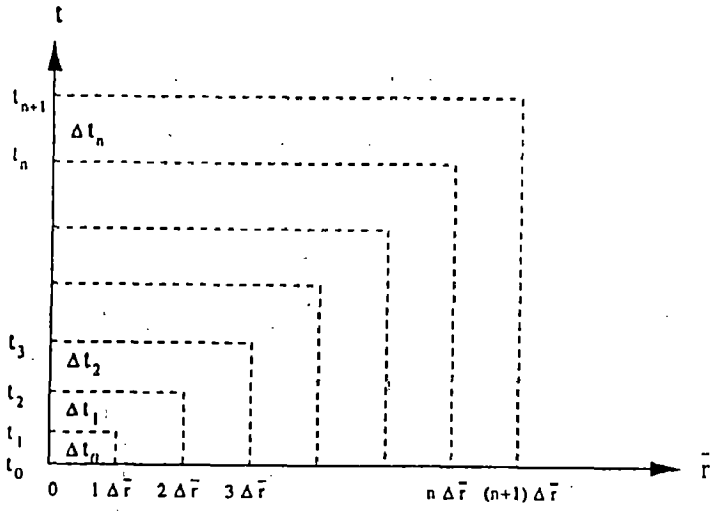

Fig (4.1) Subdivision of *"r – t"* domain using constant $\Delta\bar{r}$, variable Δt

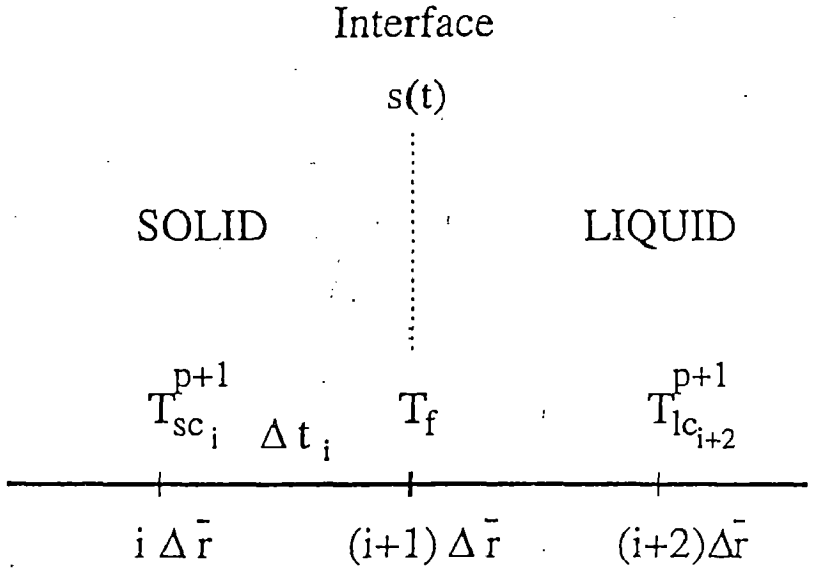

Fig (4.2) Representation of Interface at *s(t)* = (i + *1)* $\Delta\bar{r}$,

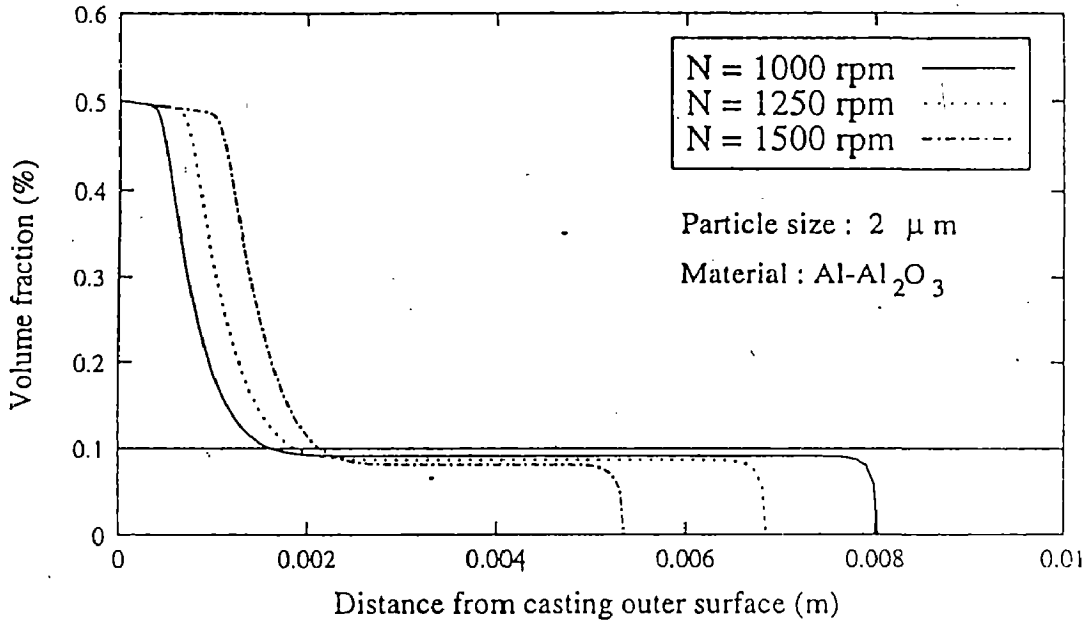

(a)

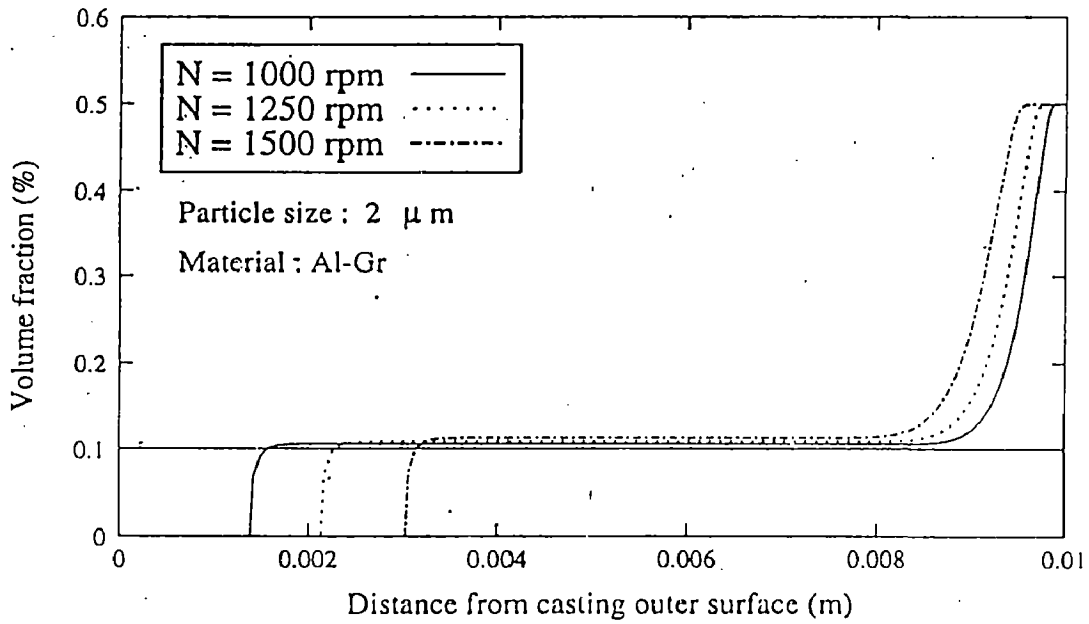

(b)

Fig (5.1) Influence of rotational speed of the casting *(N)* on the particle segregation at t = 10 sec. for (a) $\rho_p > \rho_l$ (b) $\rho_p < \rho_l$

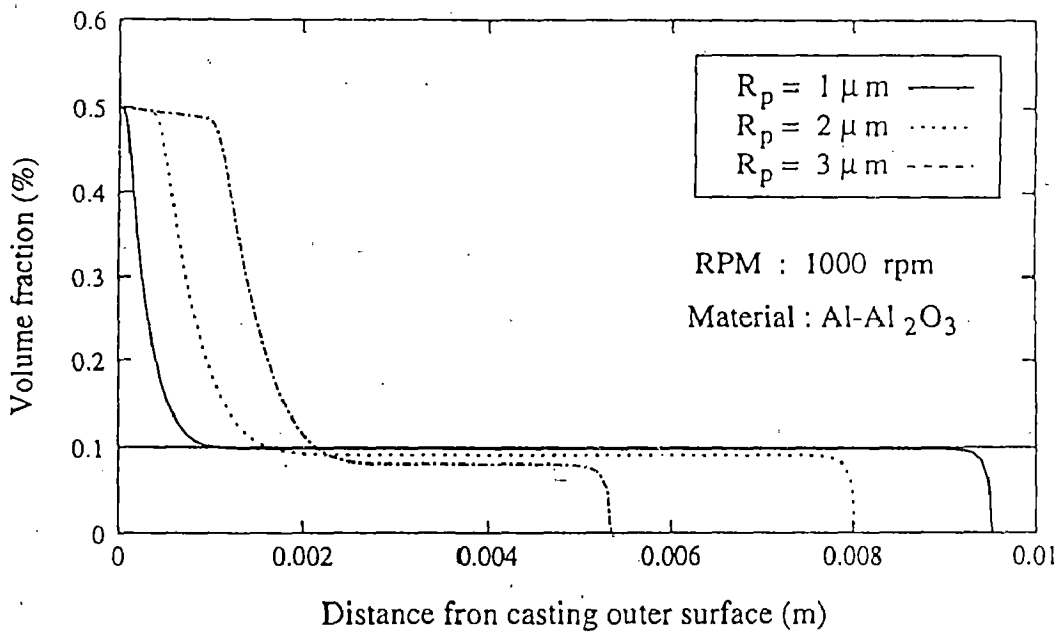

(a)

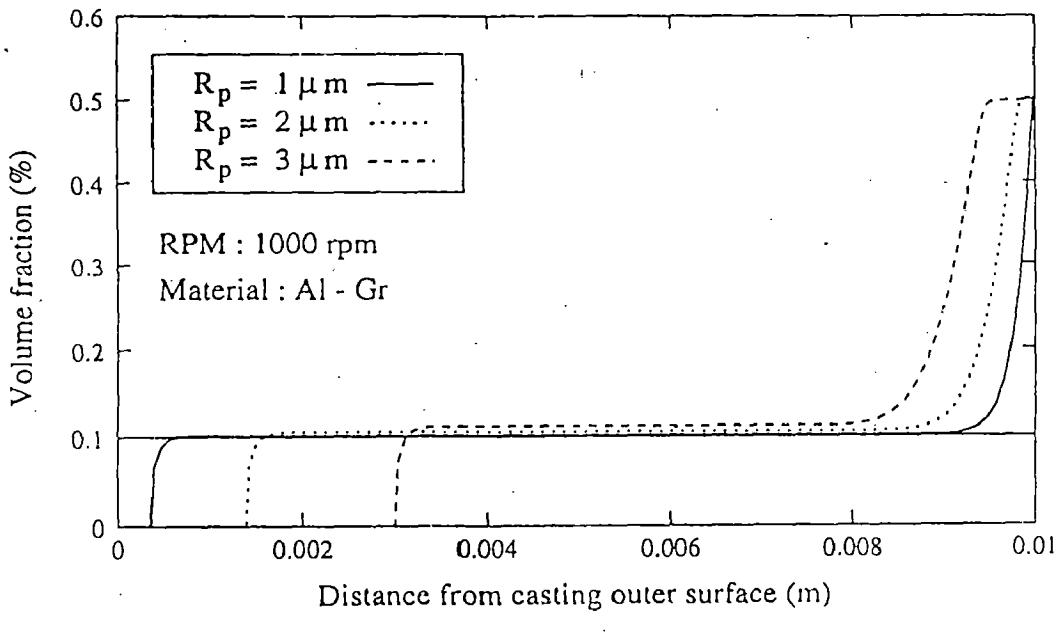

(b)

Fig (5.2) Influence of particle size (R_p) on the particle segregation at t = 10 sec. for (a) $\rho_p > \rho_l$ (b) $\rho_p < \rho_l$

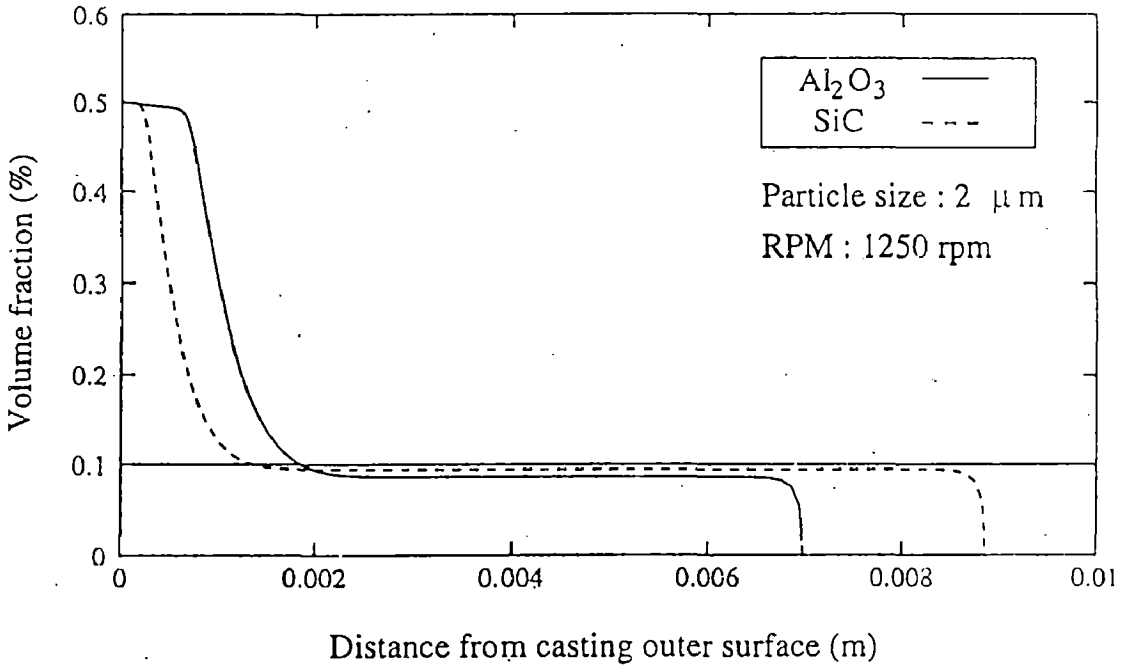

Fig (5.3) Influence of relative density difference $(\rho_p - \rho_l)$ on the particle segregation at t = 10 sec.

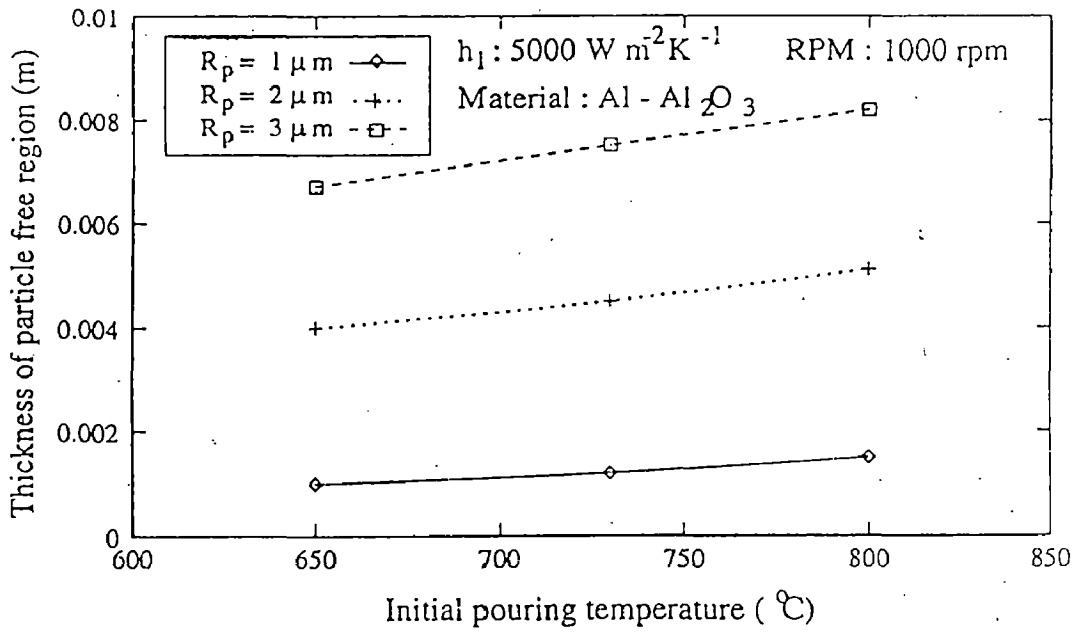

Fig (5.4) Influence of initial pouring temperature (T_p) on the variation of thickness of particle free region of Al -Al_2O_3 composite

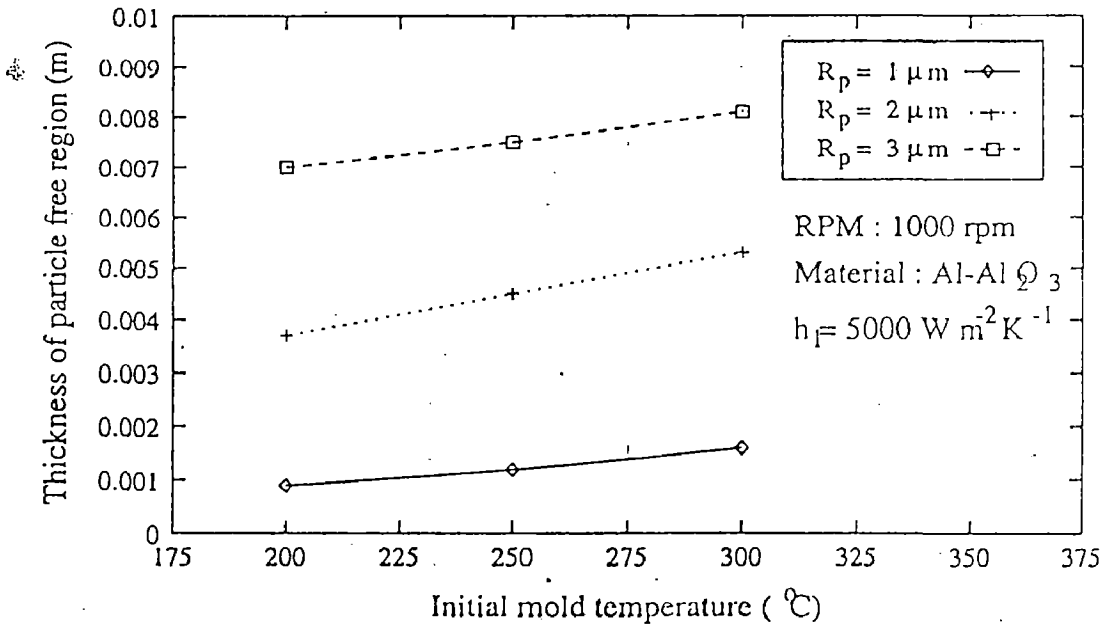

Fig (5.5) Influence of initial mold temperature *(T_M)* on the variation of particle free thickness of region of *Al -Al_2O_3* composite

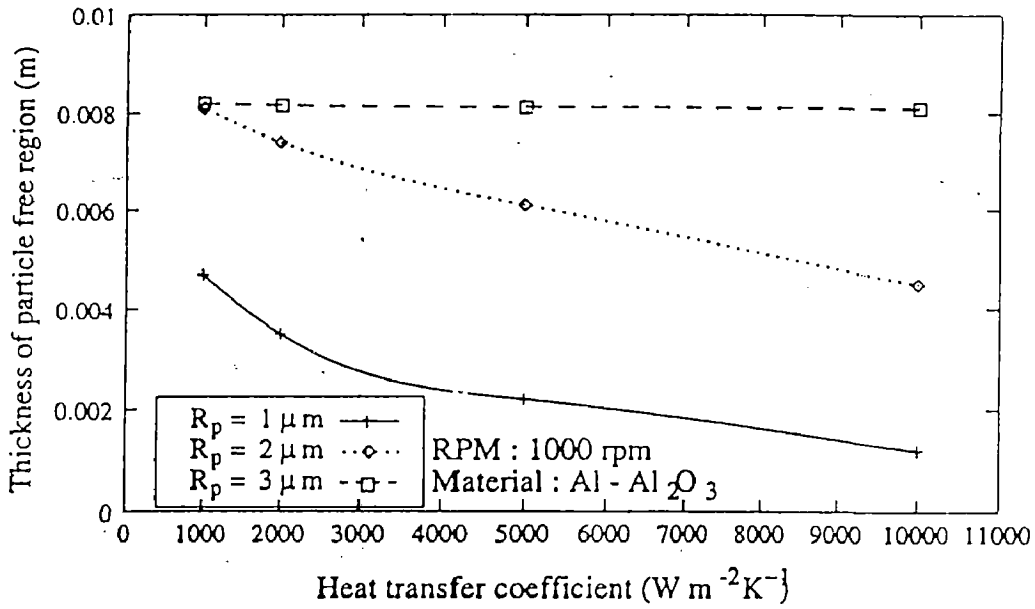

Fig (5.6) Influence of heat transfer coefficient between metal-mold interface*(h_1)* on the variation of thickness of particle free region *of Al -Al_2O_3* composite

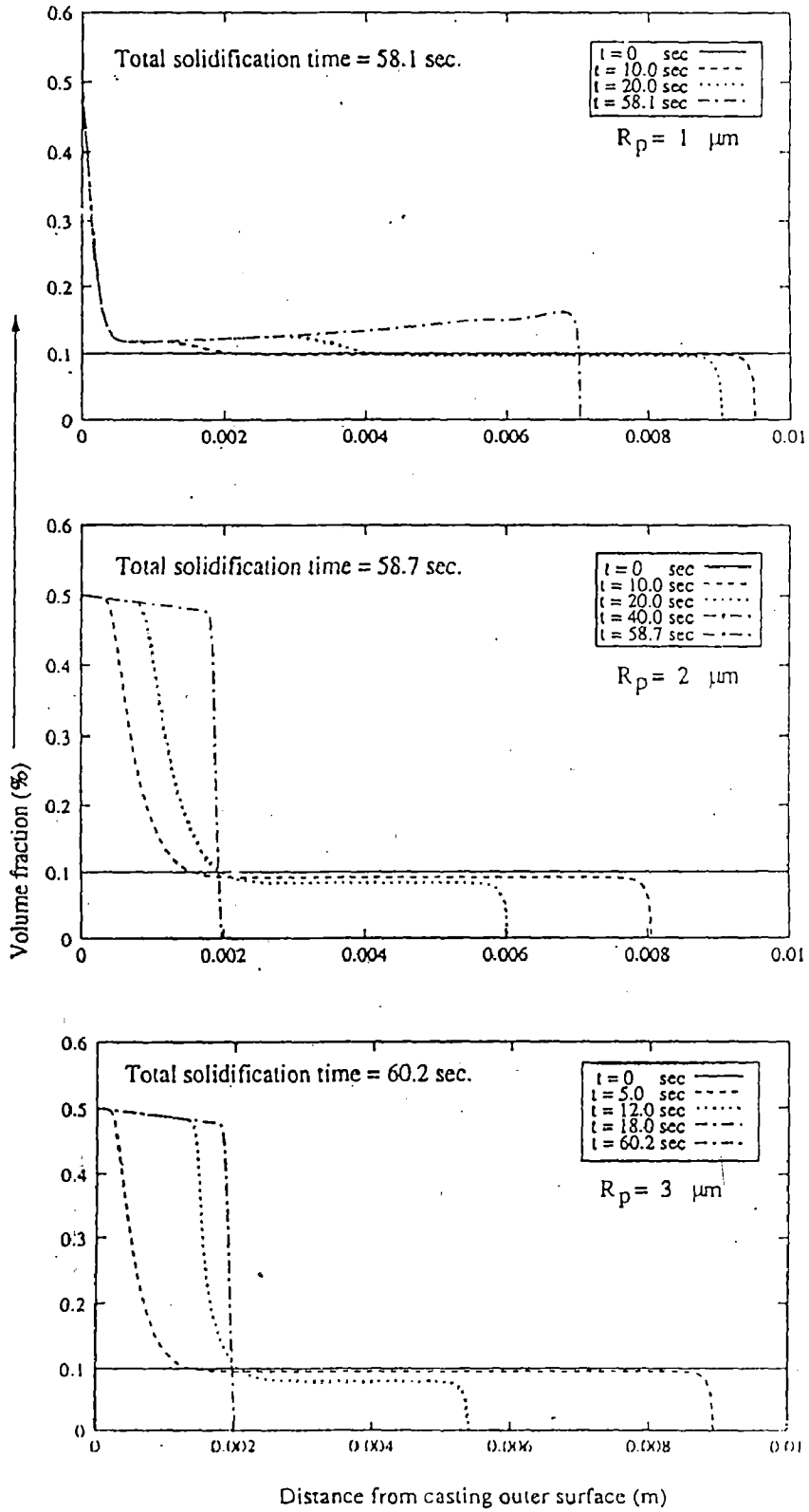

Fig (5.7) Variation of volume fraction with time for different values of R_p at h_1 = 2000 W m^{-2} K^{-1} of *Al -Al_2O_3* composite

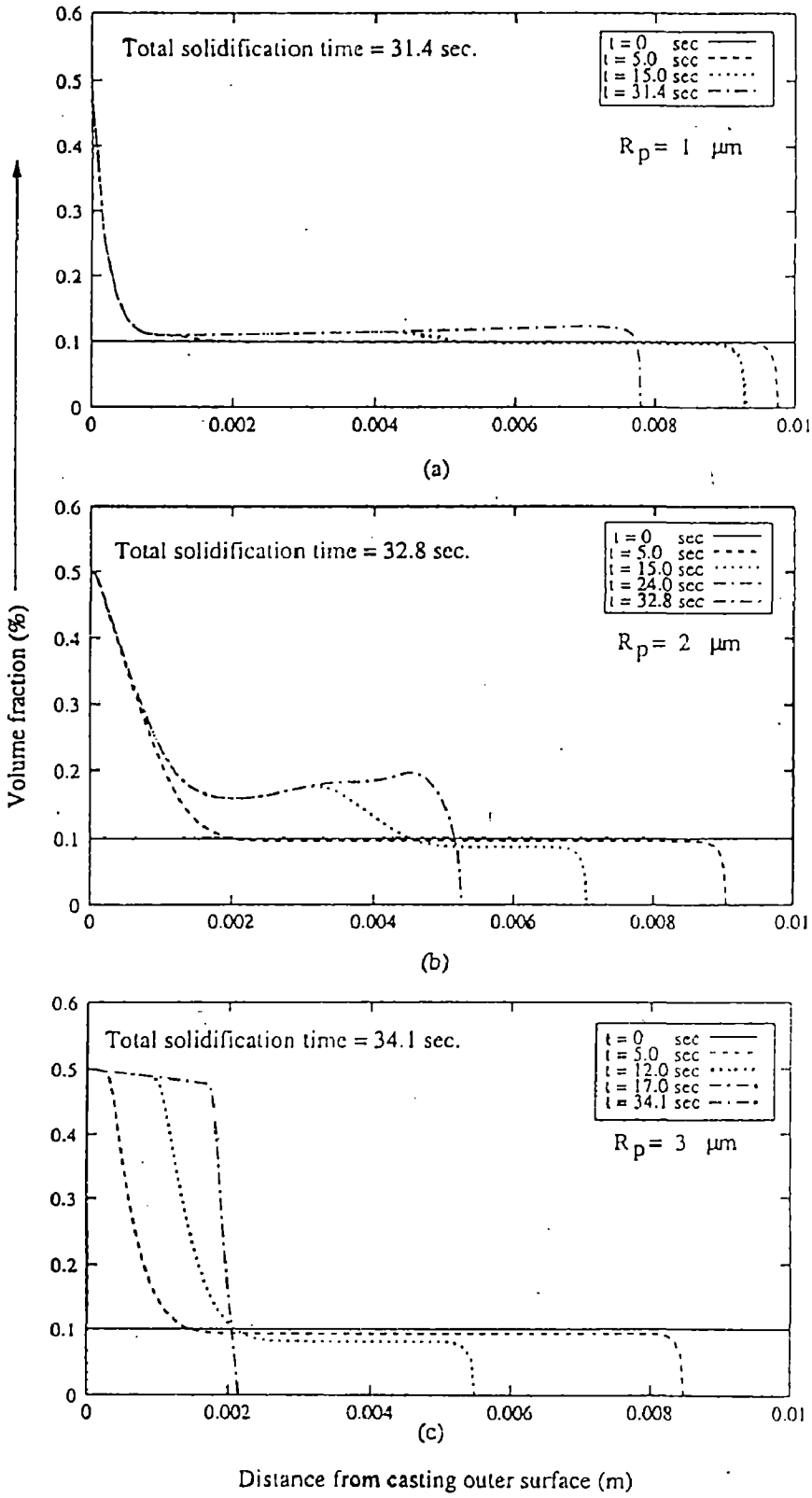

Fig (5.8) Variation of volume fraction with time for different values of R_p at h_i = 5000 $W m^{-2} K^{-1}$ of Al -Al_2O_3 composite

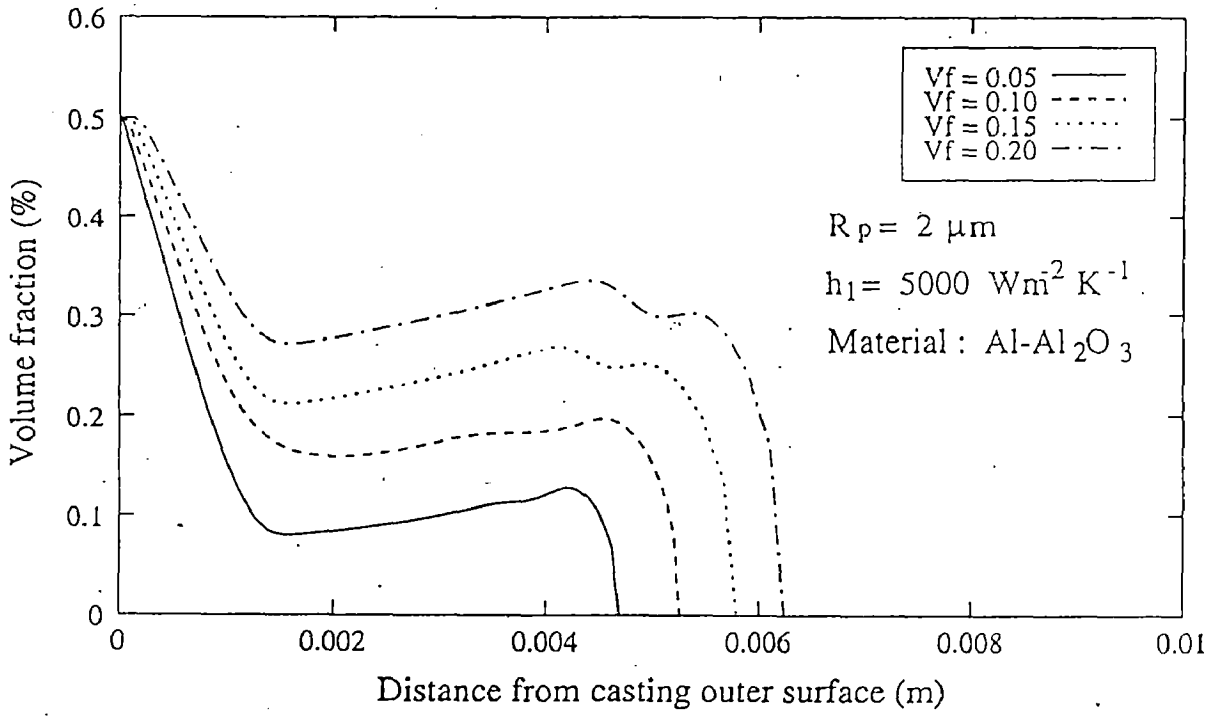

Fig (5.9) Variation of volume fraction and particle rich region thickness with initial particulate volume fraction

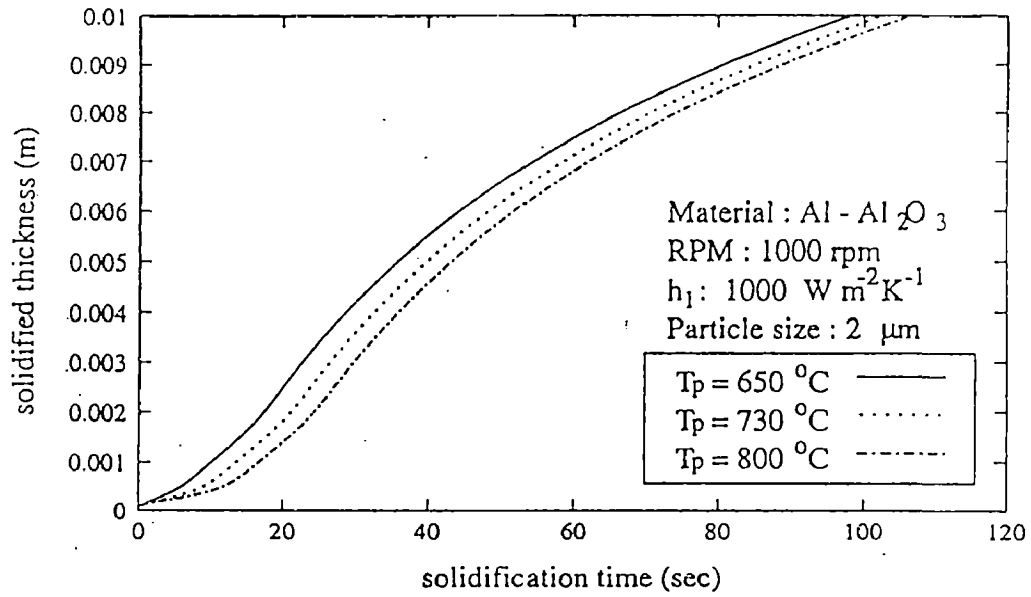

Fig (5.10) Development of the solid shell thickness as a function of solidification time for different initial pouring temperatures

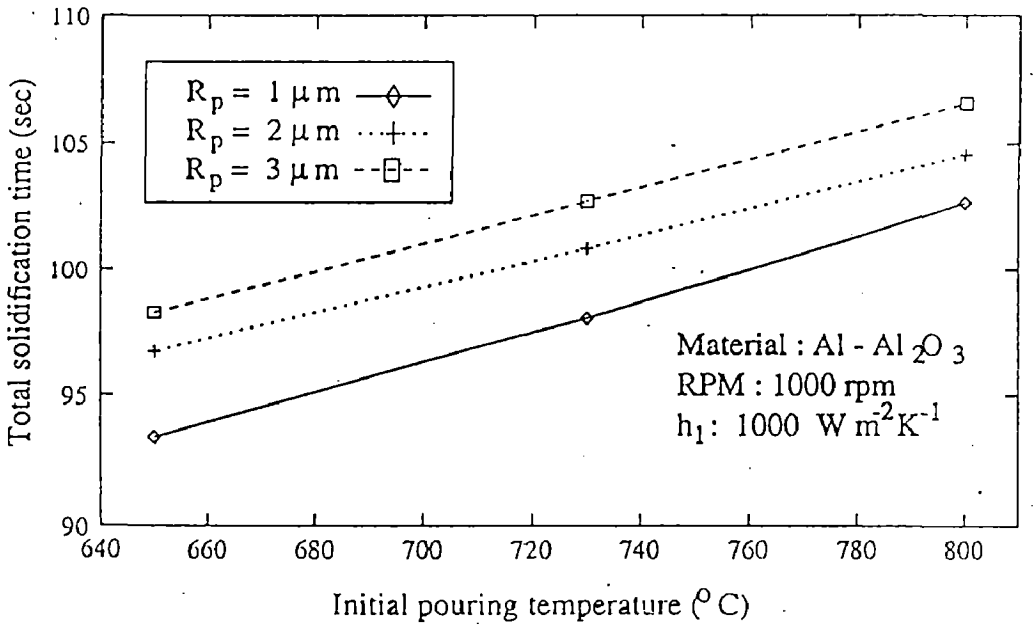

Fig (5.11) Variation of total solidification time as a function of initial pouring temperature (T_p) of *Al -Al_2O_3* composite for different values of R_p

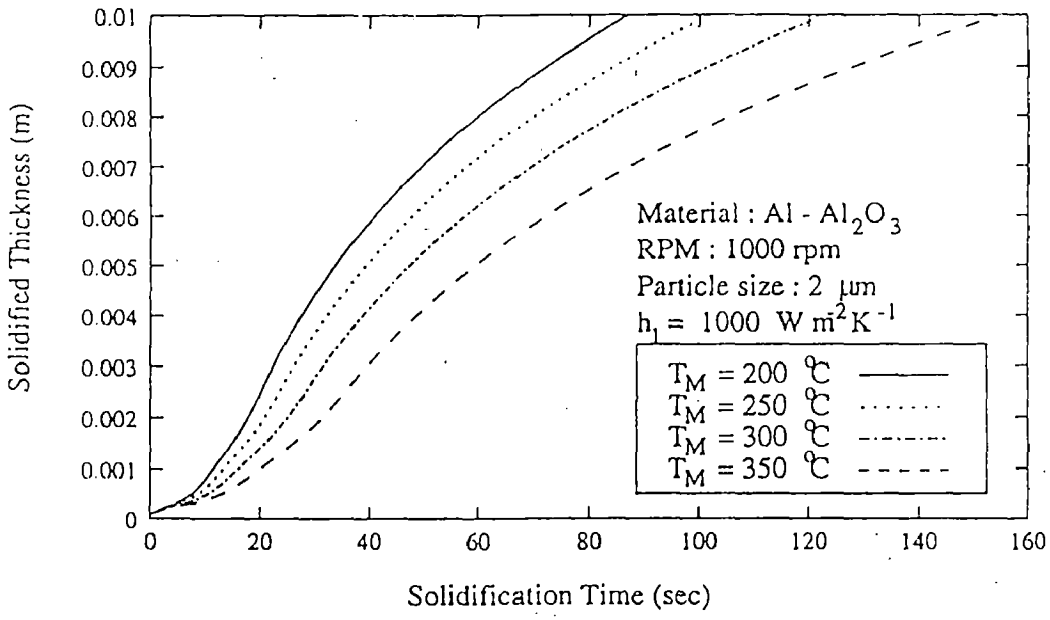

Fig (5.12) Development of the solid shell thickness as a function of solidification time for different initial mold temperatures

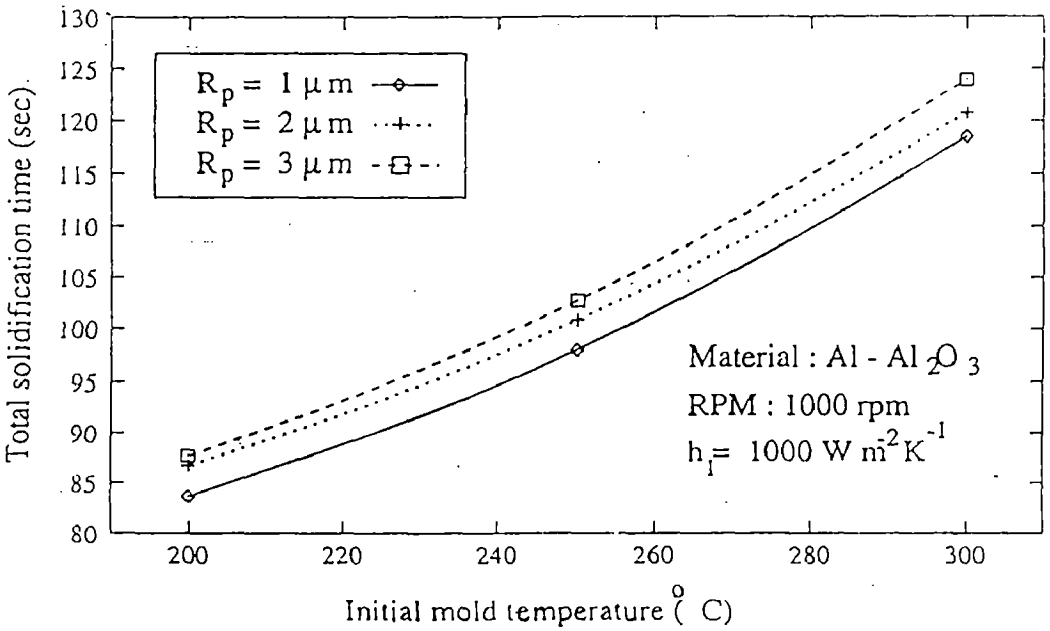

Fig (5.13) Variation of total solidification time as a function of initial mold temperature (T_M) of Al -Al_2O_3 composite for different values of R_p

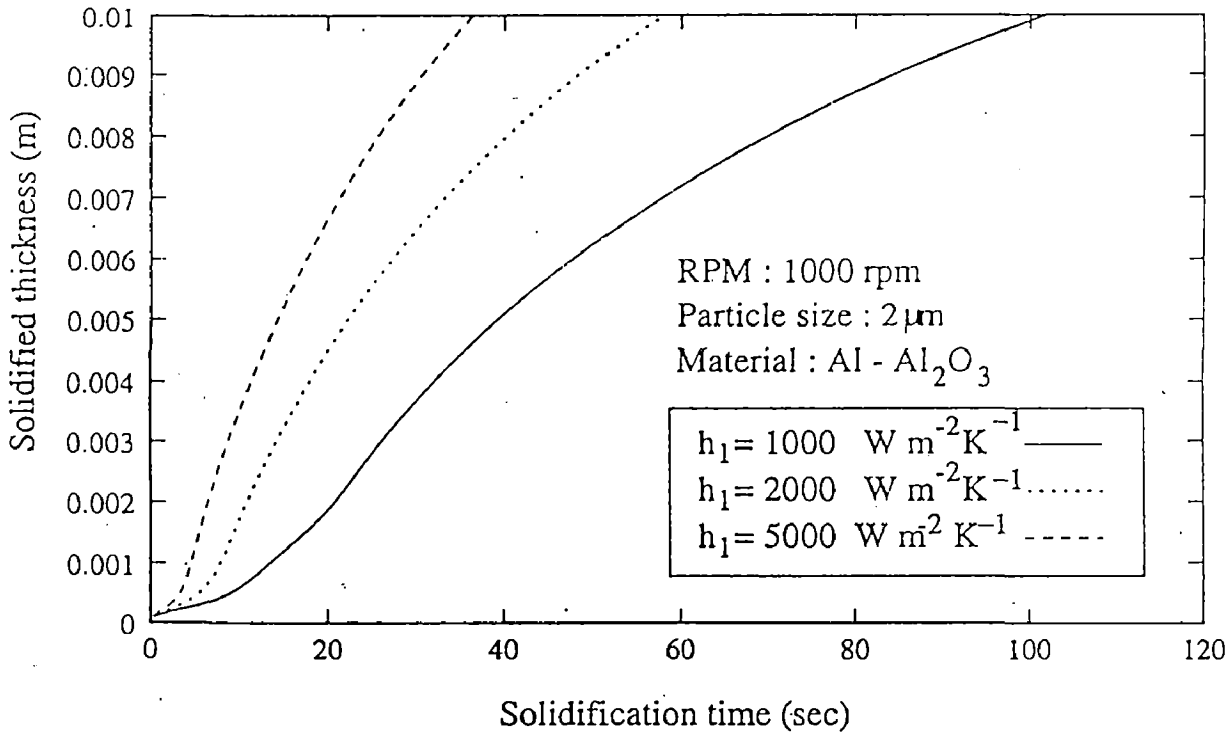

Fig (5.14) Development of the solid shell thickness as a function of solidification time for different values of h_1

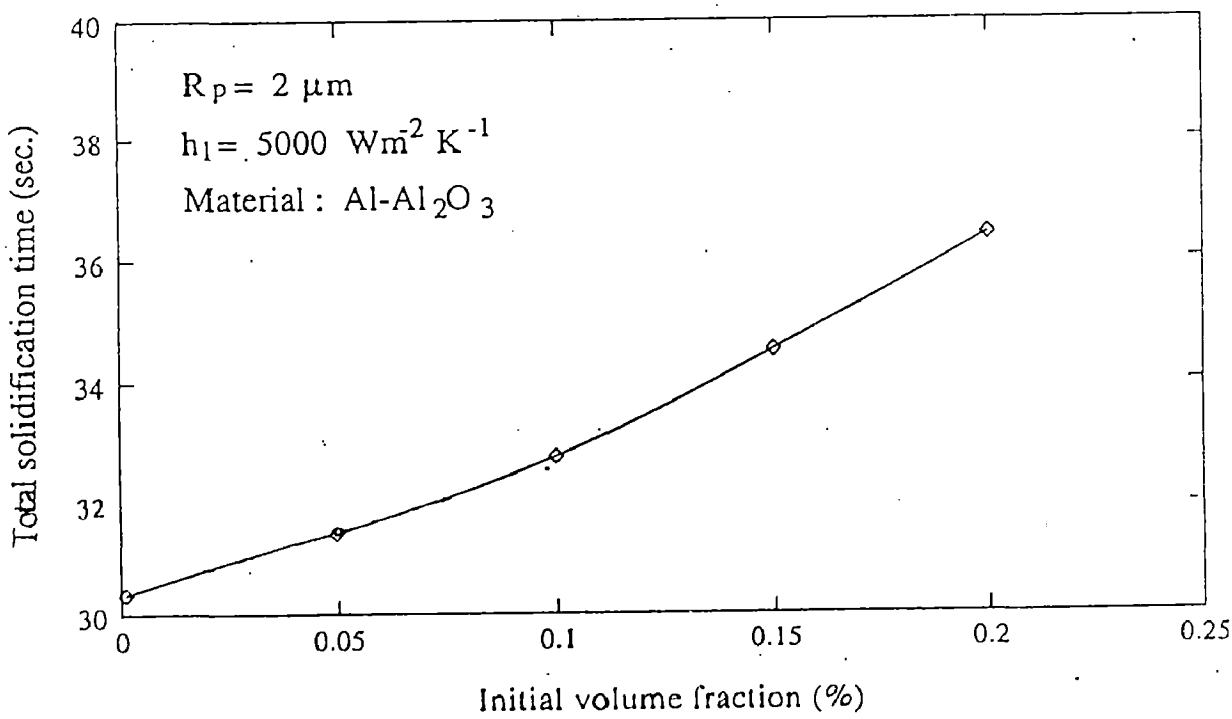

Fig (5.15) Variation of total solidification time with the particulate initial volume fraction

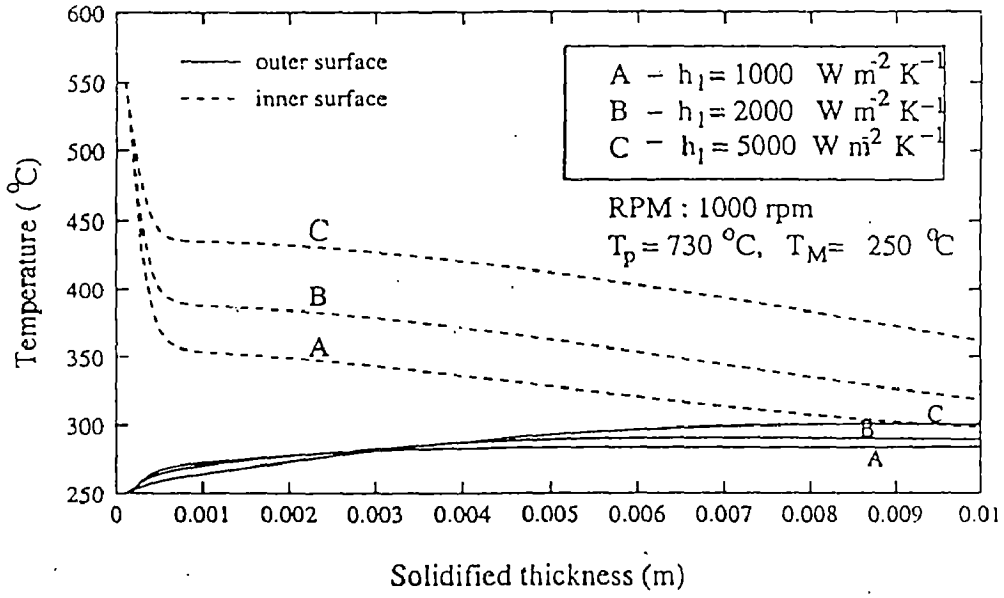

Fig (5.16) Variation of temperature at the inner and outer surface of the mold as a function of thickness of solid shell developed for different values of h_1

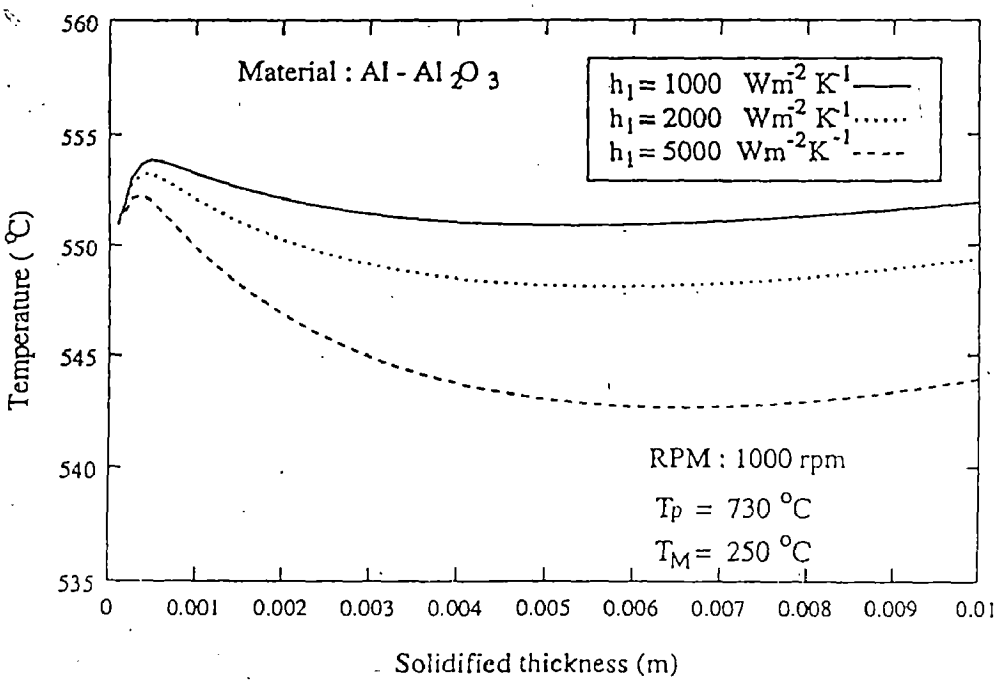

Fig (5.17) Variation of temperature at the outer surface of the casting as a function of thickness of solid shell developed for different values of h_1

APPENDIX A

INITIAL TEMPERATURE DISTRIBUTION

In order to find the metal-mold interface temperature at time t=0, the mold is assumed to be at a temperature T_M and the initial metal temperature is assumed to be the temperature of the metal as it enters the mold cavity. To find a reasonable approximation to the initial interface temperature, consider an adiabatic system shown in Fig. A-1.

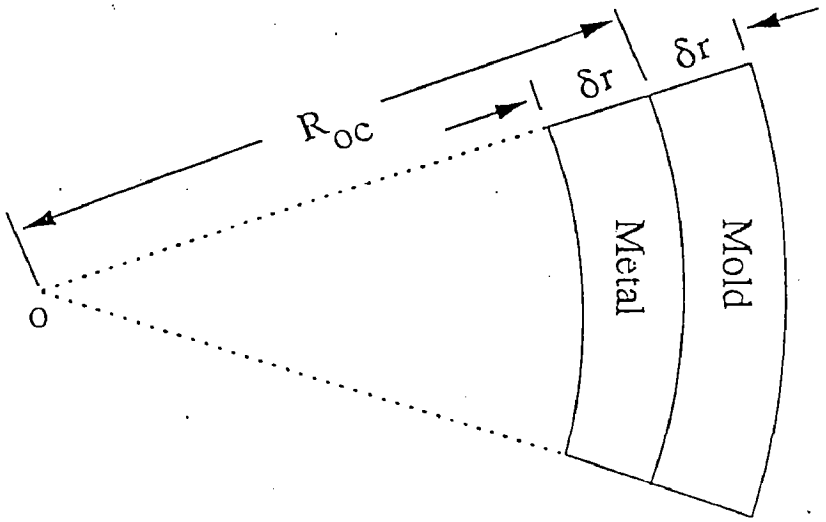

A.1 Control volume considered when calculating the initial temperature of metal-mold interface

The thermal energy initially contained in this system is $2\pi R_{oc}\delta r (\rho_g C_g T_M + \rho_{lc} C_{lc} T_p)$. The system is allowed to come to equilibrium adiabatically. The adiabatic assumption is reasonable because as $\delta \rightarrow 0$ whatever happens to the system, it is assumed to happen instantly. Also, by definition of this condition, no heat flux has yet been established, hence no heat is transferred to or from the system. Depending upon the relative values of ρ_g, ρ_{lc}, C_g, C_{lc}, T_M, T_p, and the heat of fusion of the metal *(H)*, there are three possible final states of the system.

Case I: **None of the metal solidifies.**

Equating the thermal energy in the system initially to that in the system at equilibrium yields

$$2\pi R_{oc}\delta r\,(\rho_g C_g T_M + \rho_{lc} C_{lc} T_p) = 2\pi R_{oc}\delta r\,(\rho_g C_g + \rho_{lc} C_{lc}) T_I \qquad (A.1)$$

where T_I is the initial metal-mold interface temperature. On rearranging the terms the interface temperature can be written as

$$T_I = \frac{\rho_g C_g T_M + \rho_{lc} C_{lc} T_p}{\rho_g C_g + \rho_{lc} C_{lc}} \qquad (A.2)$$

Case II: **All of the metal solidifies.**

The thermal energy released when metal solidifies is

$$2\pi R_{oc}\delta r\,(\rho_{lc} H) \qquad (A.3)$$

Conservation of energy yields

$$2\pi R_{oc}\delta r\,(\rho_g C_g T_M + \rho_{lc} C_{lc} T_p) + 2\pi R_{oc}\delta r\,(\rho_{lc} H) = 2\pi R_{oc}\delta r\,(\rho_g C_g + \rho_{lc} C_{lc}) T_I \qquad (A.4)$$

On rearranging terms, T_I can be written as

$$T_I = \frac{\rho_g C_g T_M + \rho_{lc} C_{lc} T_p + \rho_{lc} H}{\rho_g C_g + \rho_{lc} C_{lc}} \qquad (A.5)$$

Case III: **The metal partially solidifies.**

If the liquidus and solidus lines of a binary system are approximated by straight lines the fraction of the liquid solidified as a function of temperature can be expressed as

$$FS = \frac{T_L - T}{T_L - T_f} \tag{A.6}$$

where T_L and T_f are the liquidus and solidification front temperatures, respectively. Equating thermal energy in the system initially to that in the system at equilibrium yields

$$2\pi R_{oc}\delta r\left[\left(\rho_g C_g T_M + \rho_{lc} C_{lc} T_p\right) + \rho_{lc} H \frac{T_L - T_I}{T_L - T_f}\right] = 2\pi R_{oc}\delta r\left(\rho_g C_g + \rho_{lc} C_{lc}\right) T_I \tag{A.7}$$

On rearranging terms, T_I can be written as

$$T_I = \frac{\rho_g C_g T_M + \rho_{lc} C_{lc} T_p + \dfrac{T_L \rho_{lc} H}{T_L - T_f}}{\rho_g C_g + \rho_{lc} C_{lc} + \dfrac{\rho_{lc} H}{T_L - T_f}} \tag{A.8}$$

it is necessary to assume the final state of the metal (liquid, mushy, or solid) in order to determine the initial interface temperature. After estimating T_I using the appropriate equation according to the assumed condition, its value is checked to ensure that the calculated T_I falls within the temperature range initially assumed.

APPENDIX B

FINITE DIFFERENCE APPROXIMATION

The differential equations and the boundary conditions for the both mold and the casting regions can be discretized by using implicit method with the central difference scheme. To approximate the differential equations in finite difference form, a network of mesh size Δr is constructed over a region which is shown in fig. B.1

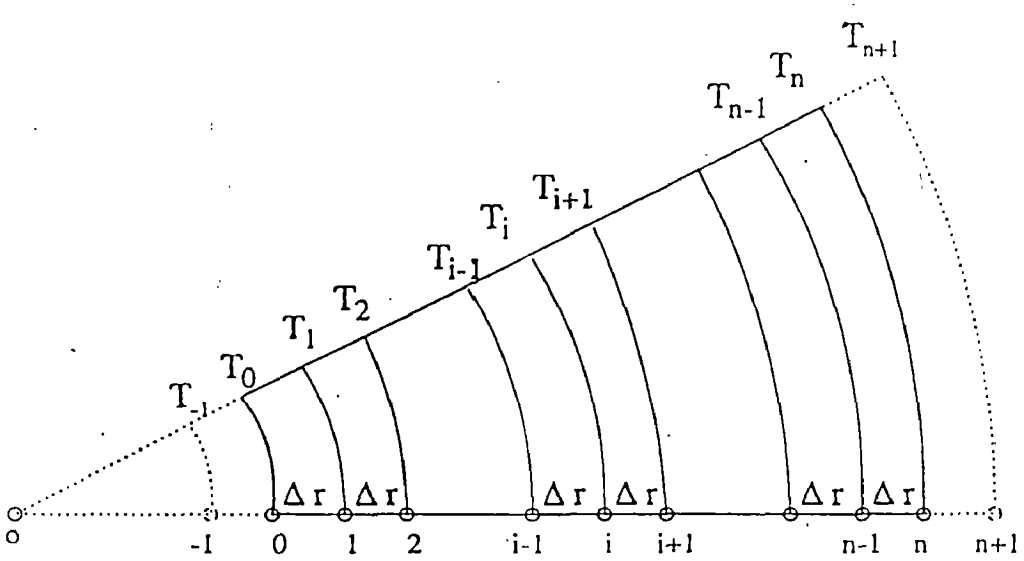

B.1 Nomenclature for finite difference representation for hollow cylinder

The thickness of each mold region subdivided into n equal grids but for casting region the total casting thickness is subdivided into n equal grids. The number of grids in the solid and the liquid composite regions vary with time. That means for the solid composite region the number of grids (n_i) goes on increasing as the solidification proceeds and for the liquid composite region the number of grids $(n-n_i)$ decreases, but their sum always remains the same as n

Steel Mold Region:

Equation (2.1) for the steel mold region is discretized as

$$\frac{T_{m_i}^{P+1} - T_{m_i}^{P}}{\Delta t} = \alpha_m \left[\frac{T_{m_{i-1}}^{P+1} - 2T_{m_i}^{P+1} + T_{m_{i+1}}^{P+1}}{(\Delta r_m)^2} + \frac{1}{R_{im} + i\Delta r_m} \frac{T_{m_{i+1}}^{P+1} - T_{m_{i-1}}^{P+1}}{2\Delta r_m} \right] \tag{B.1}$$

where

$$\Delta r_m = \frac{R_{om} - R_{im}}{n} \tag{B.2}$$

equation (B.1) is rearranged in the following form

$$-r_m \left(1 - \frac{0.5}{\frac{R_{im}}{\Delta r_m} + i} \right) T_{m_{i-1}}^{P+1} + (1 + 2r_m) T_{m_i}^{P+1} - r_m \left(1 + \frac{0.5}{\frac{R_{im}}{\Delta r_m} + i} \right) T_{m_{i+1}}^{P+!} = T_{m_i}^{P} \tag{B.3}$$

where

$$r_m = \frac{\alpha_m \Delta t}{(\Delta r_m)^2} \tag{B.4}$$

At the outer surface of the steel mold the boundary condition Eq. (2.17) is discretized as

$$-k_m \frac{T_{m_{n+1}}^{P+1} - T_{m_{n-1}}^{P+1}}{2Dr_m} = h_3 \left(T_{m_n}^{P+1} - T_\alpha \right) \tag{B.5}$$

The temperature term corresponding to the fictitious node n+1 can be eliminated by combining Eq. (B.3) at node n and Eq. (B.5). This results in the equation corresponding to the outer surface of the steel mold, i.e., at the node n, in the following form:

$$-2r_m T_{m_{n-1}}^{P+1} + \left[1 + 2r_m + K_1 r_m \left(1 + \frac{0.5}{\frac{R_{im}}{\Delta r_m} + i} \right) \right] T_{m_n}^{P+1} = K_1 r_m \left(1 + \frac{0.5}{\frac{R_{im}}{\Delta r_m} + i} \right) T_\alpha + T_{m_n}^{P} \tag{B.6}$$

where

$$-K_m = \frac{2h_3 \Delta r_m}{K_m}$$

(B.7)

Similarly for the inner surface of the steel mold the boundary condition Eq. (2.16) is discretized as

$$-K_m \frac{T_{m_1}^{P+1} - T_{m_{-1}}^{P+1}}{2\Delta r_m} = h_3 \left(T_{g_n}^{P+1} - T_{m_0}^{P+1} \right) \qquad \text{(B.8)}$$

By eliminating temperature term corresponding to the fictitious node –1 through Eq. (B.3) at node 0 and the boundary condition Eq. (B.8), the equation at the inner surface of the steel mold is obtained as

$$-K_2 r_m \left(1 - \frac{0.5}{\frac{R_{im}}{\Delta r_m} + i} \right) T_{g_n}^{P+1} + \left[1 + 2r_m + K_2 r_m \left(1 - \frac{0.5}{\frac{R_{im}}{\Delta r_m} + i} \right) \right] T_{m_0}^{P+1} - 2r_g T_{m_1}^{P+1} = T_{m_o}^{P}$$

(B.9)

where

$$K_2 = \frac{2h_4 \Delta r_m}{k_m} \qquad \text{(B.10)}$$

Graphite Mold Region :

Equation (2.1) for the graphic mold region can be discretized as

$$\frac{T_{g_i}^{P+1} - T_{g_i}^{P}}{\Delta t} = \alpha_g \left[\frac{T_{g_{i-1}}^{P+1} - 2T_{g_i}^{P+1} + T_{g_{i+1}}^{P+1}}{(\Delta r_g)^2} + \frac{1}{R_{ig} + i\Delta r_g} \frac{T_{g_{i+1}}^{P+1} - T_{g_{i-1}}^{P+1}}{2\Delta r_g} \right] \qquad \text{(B.11)}$$

where

$$\Delta r_g = \frac{R_{og} - R_{ig}}{\eta} \tag{B.12}$$

Equation (B.11) is rearranged in the following form

$$-r_g\left(1-\frac{0.5}{\frac{R_{ig}}{\Delta r_g}+1}\right)T_{g_{i-1}}^{P+1}+\left(1+2r_g\right)T_{g_i}^{P+1}-r_g\left(1+\frac{0.5}{\frac{R_{ig}}{\Delta r_g}+i}\right)T_{g_{i+1}}^{P+1}=T_{g_i}^{P} \tag{B.13}$$

where

$$r_g = \frac{\alpha_g \Delta t}{\left(\Delta r_g\right)^2} \tag{B.14}$$

At the outer surface of the graphic mold the boundary condition Eq. (2.15) is discretized as

$$-k_g \frac{T_{g_{n+1}}^{P+1} - T_{g_{n-1}}^{P+1}}{2\Delta r_g} = h_4\left(T_{g_n}^{P+1} - T_{m_o}^{P+1}\right) \tag{B.15}$$

The temperature term corresponding to the fictitious node n+1 is eliminated using Eq. (B.13) at the node n and the boundary condition Eq. (B.15). The resulting equation relates to the temperature at the outer surface of the graphic mold as

$$-2r_g T_{g_{n-1}}^{P+1}+\left[1+2r_g+K_3 r_g\left(1+\frac{0.5}{\frac{R_{ig}}{\Delta r_g}+i}\right)\right]T_{g_n}^{P+1}-K_3 r_g\left(1+\frac{0.5}{\frac{R_{ig}}{\Delta r_g}+i}\right)T_{m_o}^{P+1}=T_{g_n}^{P} \tag{B.16}$$

where

$$K_3 = \frac{2h_4 \Delta r_g}{k_g} \tag{B.17}$$

Similarly the boundary condition Eq. (2.14) at the inner surface of the graphite mold can be discretized as

$$-k_g \frac{T_{g_1}^{P+1} - T_{g_{-1}}^{P+1}}{2\Delta r_g} = h_1 \left(T_{sc_0}^{P+1} - T_{g_0}^{P+1} \right) \tag{B.18}$$

The temperature corresponding to the fictitious node –1 can be eliminated by combining Eq. (B.13) at the node 0 and the corresponding boundary condition given by Eq. (B.18). The resulting equation that incorporates the inner surface of the graphite mold is

$$-K_4 r_g \left(1 - \frac{0.5}{\frac{R_{ig}}{\Delta r_g} + i} \right) T_{sc_0}^{P+1} + \left[1 + 2r_g + K_4 r_g \left(1 - \frac{0.5}{\frac{R_{ig}}{\Delta r_g} + i} \right) \right] T_{g_0}^{P+1} - 2r_g T_{g_1}^{P+1} = T_{g_0}^{P} \tag{B.19}$$

where

$$K_4 = \frac{2h_1 \Delta r_g}{k_g} \tag{B.20}$$

Solid Composite Region :

Equation (2.24) for the solid composite region can be discretized as

$$\frac{T_{sc_i}^{P+1} - T_{sc_i}^{P}}{\Delta t} = \frac{\alpha_{sc_i} \Delta t}{(s(t))^2} \frac{T_{sc_i-1}^{P+1} - 2T_{sc_i}^{P+1} + T_{sc_i+1}^{P+1}}{(\Delta \xi)^2} + \frac{1}{s(t)} \left[i \Delta \xi \frac{\Delta s(t)}{\Delta t} - \frac{\alpha_{sc\,i}}{R_{oc} - i \Delta \xi s(t)} \right] \frac{T_{sc_i+1}^{P+1} - T_{sc_i-1}^{P+1}}{2\Delta \xi} \tag{B.21}$$

where

$$\Delta\xi = \frac{1}{n_i} \tag{B.22}$$

Equation (B.21) is rearranged as

$$-r_{sc_i}\left(1-0.5A^*\right)T_{sc_i-1}^{P+1} + \left(1+2r_{sci}\right)T_{sc_i}^{P+1} - r_{sci}\left(1+0.5A^*\right)T_{sc_{i+1}}^{P+1} = T_{sc_i}^{P} \tag{B.23}$$

where

$$r_{sci} = \frac{\alpha_{sc_i}\Delta t}{\left(s(t)\Delta\xi\right)^2} \tag{B.24}$$

$$A^* = \frac{i(\Delta\xi)^2 s(t)}{\alpha_{sc_i}}\frac{\Delta s(t)}{\Delta t} - \frac{1}{\frac{R_{oc}}{\Delta\xi s(t)} - i} \tag{B.25}$$

At the outer surface of the casting the boundary condition Eq. (2.25) is discretized as

$$\frac{k_{sc_i}}{s(t)}\frac{T_{sc_i}^{P+1} - T_{sc_{i-1}}^{P+1}}{2\Delta\xi} = h_1\left(T_{sc_0}^{P+1} - T_{g_0}^{P+1}\right) \tag{B.26}$$

Eliminating the temperature term corresponding to the fictitious node –1 by combining Eq. (B.23) at node 0 and the boundary condition given Eq. (B.26) results in equation which incorporates the outer surface of the casting :

$$-K_5 r_{sc_i}\left(1-0.5A^*\right)T_{g_0}^{P+1} + \left[1+2r_{sc_i}+K_5 r_{sc_i}\left(1-0.5A^*\right)\right]T_{sc_0}^{P+1} - 2r_{sc_i}T_{sc_1}^{P+1} = T_{sc_0}^{P+1} \tag{B.27}$$

where

$$K_5 = \frac{2h_1 s(t)\Delta\xi}{k_{sc_i}} \tag{B.28}$$

Liquid Composite Region :

Equation (2.27) for liquid composite region is discretized as

$$\frac{T_{lc_i}^{P+1}-T_{lc_i}^{P}}{\Delta t}=\frac{1}{r_i-s(t)}\left[(1-i\Delta\eta)\frac{\Delta s(t)}{\Delta t}-\frac{\alpha_{lci}}{(R_{oc}-s(t))-i\Delta\eta(r_i-s(t))}\right]\frac{T_{lc_{i+1}}^{P+1}-T_{lc_{i-11}}^{P+1}}{2\Delta\eta}$$

$$+\frac{\alpha_{lci}}{(r_i-s(t))^2}\frac{T_{lc_{i-1}}^{P+1}-2T_{lc_i}^{P+1}+T_{lc_{i+1}}^{P+1}}{(\Delta\eta)^2} \qquad \text{(B.29)}$$

where

$$\Delta\eta=\frac{1}{n-n_i} \qquad \text{(B.30)}$$

Equation (B.29) can be rearranged as

$$-r_{lci}(1-0.5B^*)T_{lc_{i-1}}^{P+1}+(1+2r_{lci})T_{lc_i}^{P+1}-r_{lci}(1+0.5B^*)T_{lc_{i+1}}^{P+1}=T_{lc_i}^{P} \qquad \text{(B.31)}$$

where

$$r_{lc_i}=\frac{\alpha_{lci}\Delta t}{((r_i-s(t))\Delta\eta)^2} \qquad \text{(B.32)}$$

$$B^*=\frac{(1-i\Delta\eta)\Delta\eta(r_i-s(t))}{\alpha_{lci}}\frac{\Delta s(t)}{\Delta t}-\frac{1}{\frac{R_{oc}-s(t)}{\Delta\eta(r_i-s(t))}-i} \qquad \text{(B.33)}$$

At the inner surface of the casting the boundary condition Eq. (2.29) is discretized as

$$\frac{-k_{lci}}{r_i-s(t)}\frac{T_{lc_{n+1}}^{P+1}-T_{lc_{n-1}}^{P+1}}{2\Delta\eta}=h_2\left(T_{lc_n}^{P+1}-T_{\beta}\right) \qquad \text{(B.34)}$$

The temperature term corresponding to the fictitious node n+1 is eliminated by combining Eq. (B.31) at node n and the boundary condition Eq. (B.34), resulting in the equation incorporating the inner surface of the casting as

$$-2r_{lci}T_{lc_{n-1}}^{P+1}+\left(1+2r_{lc_i}+K_6 r_{lci}(1+0.5B^*)\right)T_{lc_n}^{P+1}=K_6 r_{lci}\left(1+0.5B^*\right)T_\beta+T_{lc_n}^{P} \qquad \text{(B.35)}$$

where

$$K_6=\frac{2h_2\Delta\eta(r_i-s(t))}{k_{lc_i}} \qquad \text{(B.36)}$$

At Solid-Liquid Interface :

Equations (2.26) and (2.28), representing the condition of continuity of temperature at the interface, are written as

$$T_{lc_{n_i}}^{P+1}=T_{sc_{n_i}}^{P+1}=T_f \qquad \text{(B.37)}$$

Equation (2.30) representing the energy balance at the solid-liquid interface is discretized as

$$\frac{k_{sc_{n_i}}}{s(t)}\frac{T_{sc_{n_i}}^{P+1}-T_{sc_{n_i-1}}^{P+1}}{\Delta\xi}=\frac{k_{lc_{n_i}}}{r_i-s(t)}\frac{T_{lc_{n_i+1}}^{P+1}-T_{lc_{n_i}}^{P+1}}{\Delta\eta}+\rho_{sc_{n_i}}H_e\frac{\Delta s(t)}{\Delta t} \qquad \text{(B.38)}$$

Equation (B.38) is rearranged in the form

$$\Delta t=\frac{\rho_{sc_{n_i}}H_e\Delta s(t)}{k_{scn_i}}\left[\frac{1}{\frac{1}{s(t)}\frac{T_f-T_{SC_{N_i-1}}^{p+1}}{\Delta\xi}-\frac{k_{lcn_i}}{k_{scn_i}}\frac{1}{r_i-s(t)}\frac{T_{lc_{n_i+1}}^{p+1}-T_f}{\Delta\eta}}\right] \qquad \text{(B.39)}$$

Equations (B.6), (B.3), (B.9), (B.16), (B.13), (B.19), (B.27), (B.23), (B.37), (B.31) and (B.35) are arranged in the tridiagonal matrix form and the solution of these equations is obtained by using the Thomas Algorithm (TDMA). This results in temperature distribution in both the casting and the mold regions for a particular time step Δt_n.